NASA TM X-506

TECHNICAL MEMORANDUM

X-506

FLOW SEPARATION ON ELLIPSOIDAL-NOSED CYLINDER-FLARE MODELS AT TRANSONIC MACH NUMBERS

By Joseph W. Cleary

Ames Research Center
Moffett Field, Calif.

NATIONAL AERONAUTICS AND SPACE ADMINISTRATION

WASHINGTON

May 1961

NATIONAL AERONAUTICS AND SPACE ADMINISTRATION

TECHNICAL MEMORANDUM X-506

FLOW SEPARATION ON ELLIPSOIDAL-NOSED CYLINDER-FLARE MODELS AT TRANSONIC MACH NUMBERS*

By Joseph W. Cleary

SUMMARY

Wind-tunnel tests were conducted of oblate ellipsoidal-nosed cylinder-flare models to investigate the onset of flow separation at Mach numbers near critical. The results showed that if the nose were sufficiently blunt, separation would occur at what is believed a subcritical Mach number at 0° angle of attack. At slightly supercritical Mach numbers, weak shocks formed near the nose-body juncture. Separation was induced by either increasing angle of attack at constant Mach number or increasing Mach number at constant angle of attack.

The effect of removing boundary layer by applying a small amount of suction locally near the nose-body juncture was investigated. With the small amount of suction applied, the shock pattern observed is believed representative of that for attached flow and the peak negative pressure coefficients were increased.

The peak negative pressure coefficients of models having attached flow with or without suction were empirically correlated for Mach numbers near 1.0. This correlation, together with experimentally determined separation boundaries, was used in estimating the angle of attack for transonic flow separation of ellipsoidal-nosed models.

INTRODUCTION

The detrimental effect of flow separation at transonic Mach numbers on the static and dynamic stability characteristics of blunt-nosed cylinder-flare models has been investigated in references 1, 2, and 3. The results of references 2 and 3 showed that dynamic instability due to either a nonconservative restoring force or negative damping would not occur if nose bluntness was not extreme. It was observed in reference 2 that the

*Title, Unclassified

separation was related to the presence of local shocks and that shock strength should be kept to a minimum, consistent with the requirements of bluntness. In addition, the shadowgraphs of reference 2 indicated the separation was more or less periodic in nature so that shock motion might be coupled with the formation of vortices. Thus it follows that alleviating shock strength would be beneficial in reducing or eliminating transonic buffet insofar as the source of the input forces causing buffet is directly related to unsteady interaction of shock waves with the boundary layer.

As an extension of the investigation of reference 2, additional wind-tunnel static-pressure measurements were made to investigate the incipient nature of the separation phenomena at Mach numbers near critical. Tests were made of the effectiveness of removing boundary layer to control the separated flow by applying suction locally near the nose-body juncture.

NOTATION

C_p	pressure coefficients, $\frac{p_l - p}{q}$
$C_{p_{cr}}$	critical pressure coefficient
d	cylindrical-body diameter
d_1	flare base diameter
l	length of cylindrical body and flare
M	free-stream Mach number
M_{cr}	critical Mach number
p_l	local static pressure
p	free-stream static pressure
q	free-stream dynamic pressure
r	nose ordinate
R	Reynolds number based on d
x	distance from nose-body juncture
w_a	air mass-flow rate per unit area
α	angle of attack

τ nose thickness, $\frac{d/2}{\lambda}$

λ nose length

γ ratio of specific heats

Subscript

s separation

MODELS, TESTS AND PRECISION

Both models were of smooth Fiberglas construction with the dimensions presented in figure 1. The model having a nose thickness $\tau = 2$ was the same oblate-nosed cylinder-flare model of reference 2. For this investigation, this model has been designated the $\tau = 2$ model to distinguish it from the blunter $\tau = \frac{1}{4}$ model shown in figure 1. Static-pressure orifices were installed flush with the model surface in the upper half of the vertical plane of symmetry. The longitudinal position of the orifices is given in table I.

A limited amount of suction was applied locally near the nose-body juncture of the $\tau = 2$ model to remove boundary-layer air and thus control the separated flow. As shown in sketch (a), suction was applied through two rows of holes. Two different arrangements of these holes were used as shown in sketch (a). Each row contained 180 holes of

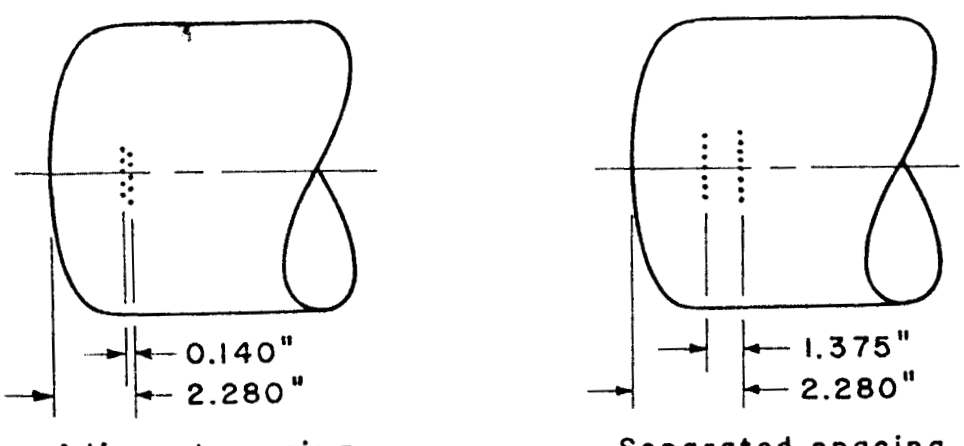

Sketch (a)

3/32-inch diameter equally spaced around the circumference of the model, to give a total open area of 2.487 square inches. The model was sealed internally and the air flowed through the sting and a rear strut to vacuum pumps exterior to the tunnel test section. The installation for tests with suction is shown in figure 2.

The air mass-flow rates through the holes and through the test section of the tunnel are given in figure 3. As shown in figure 3, the mass flow through the holes was less than the mass flow through the tunnel per unit area and since the open area of the holes was small compared to model cross-sectional area, the sink effect of removing air by suction is believed negligible. Any effects observed, therefore, are attributed primarily to boundary-layer control. Although the local effect of the proximity of suction holes to pressure orifices is not known, it is believed small because the application of suction had negligible effect on the static pressure of the nearest orifice for $M = 0$.

The tests were conducted in the Ames 14-Foot Transonic Wind Tunnel at Mach numbers from 0.15 to 0.94. The Reynolds number based on model diameter was approximately as shown in figure 4. The angle of attack was from about -4° to $+20^\circ$. For tests with suction, the rigid attachment of the rear strut to the sting and tunnel wall restrained the model at 0° angle of attack.

Pressure measurements were made with mercury-in-glass manometers for Mach numbers greater than 0.50 while for lower Mach numbers, tetrabromoethane was used. Pressure coefficients are believed precise within ± 0.020.

RESULTS AND DISCUSSION

The results of reference 2 showed at 0° angle of attack the flow of the $\tau = 2$ oblate-nosed model was separated at a supercritical Mach number of 0.60 whereas at a subcritical Mach number of 0.40 the flow was attached. Since separation was occurring at a Mach number near the critical, it was suggested in reference 2 that separation was shock induced. However, separation altered the flow to such an extent that the flow was only slightly supercritical and the presence of shocks barely discernible. In order to examine the origin of the separated flow in greater detail, additional tests were made at subcritical and slightly supercritical Mach numbers.

Typical effects of Mach number and angle of attack on the flow and pressure distribution are presented in figures 5 and 6, respectively. Peak negative pressure coefficients and separation boundaries obtained from these data, reference 2, and data with suction (to be presented

later) are plotted in figure 7 as a function of Mach number. The separation boundaries shown in figure 7 represent the peak negative pressure coefficient achieved before flow separation ensued.

At 0° angle of attack and 0.50 Mach number, the flow was slightly supercritical as indicated by figure 7, and although weak shocks are visible near the nose-body juncture in figure 5(a), the flow remained attached. At this Mach number, observations of the flow during the test indicated local shock strength was increased by either increasing angle of attack at constant Mach number or increasing Mach number at constant angle of attack. In either case the flow separated when shock strength was sufficiently increased, creating a new stable flow for which weak shocks were barely discernible. Some indication of the effect observed of increasing Mach number on shock strength with the flow remaining attached can be obtained by comparing the shadowgraph of figure 5(a) at 0.50 Mach number with that of figure 10(a) at 0.60 Mach number with suction applied.

Figure 7 shows the angle of attack and the peak negative pressure coefficient for which separation occurred increased with increasing Mach number at subcritical Mach numbers and decreased with increasing Mach number at Mach numbers greater than critical. The separation at angle of attack at subcritical Mach numbers was apparently a low-speed stall. Since Reynolds number increased almost directly with Mach number in the lower Mach number range (see fig. 4), the relative importance of increasing Mach or Reynolds number in delaying separation could not be established. It is clear, however, the favorable effect of increasing Mach and/or Reynolds number in delaying separation in the subcritical range did not exist at supercritical Mach numbers.

Tests were made of the $\tau = 4$ model which was expected to have a much lower critical Mach number than the $\tau = 2$ model. The results showing the effect of Mach number at 0° angle of attack and the effect of angle of attack at 0.40 Mach number are given in figures 8 and 9, respectively. It is evident from both the shadowgraphs and pressure distributions of figure 8 that the flow was separated even at the lowest Mach number of the test, 0.165, and therefore, the critical Mach number, if the flow were attached, could not be determined. An estimate was made of the peak negative pressure coefficient for attached flow at a Mach number of 0.165 and 0° angle of attack by an extrapolation of the correlation of peak negative pressures presented in reference 2, figure 24. The critical pressure coefficient for a Mach number of 0.165 is -24 and this value numerically exceeds the extrapolated value (estimated for $\tau = 4$) by a factor greater than 5. Since it appears unlikely the estimate would be off by such a large factor, it was concluded that if the flow were attached it would be subcritical at a Mach number of 0.165 but the peak pressure would be well above the separation boundary shown in figure 7.

Effect of Suction

Pressure distributions and shadowgraphs showing the effect of suction on flow separation are presented in figure 10 for Mach numbers from 0.60 to 0.94. Pressure data have been omitted for clarity where the effects were small. Also not shown are pressure data obtained without suction but with suction holes open; except for a reduction in the peak negative pressure coefficient, these data were similar to pressure distributions without suction holes shown in figure 10.

It is apparent from shadowgraphs of figure 10 that if separation occurred, suction reduced the extent of separated flow and the resulting shock pattern was more nearly representative of that for unseparated flow. Moreover, the separation does not appear periodic in nature and the presence of ring vortices is not apparent. The main effect on the pressure distributions was an increase in the peak negative pressure coefficient and, at higher Mach numbers, a better pressure recovery over the full length of the model. At Mach numbers of 0.90 and 0.94, the pressure distributions indicate the separated spacing of the hole rows was more effective in preventing separation than was the adjacent spacing. Since, at these Mach numbers, the mass flow rate was about the same for both spacings of the rows as shown in figure 3, it was concluded that the greater effectiveness of the separated spacing was due to better distribution of suction. The shadowgraphs of figures 10(e) and 10(g) for Mach numbers of 0.90 and 0.94, respectively, with suction show the flow was completely attached over the nose and the forward part of the cylindrical body but the boundary layer thickened over the afterportion. The thickening is attributed to the interaction of the nearly normal shock on the body with the boundary layer and creates an oblique shock (discernible in the corner of the window of figure 10(g) and intersecting the body behind the window frame, presumably at about where the boundary layer first thickens).

A 3 9 1

At a Mach number of 0.94 without suction, the flow separated at the nose-body juncture and the normal shock was slightly forward of its location with suction (see fig. 10(g)). Also, an abrupt pressure rise was not indicated by the pressure distribution at the position of the shock in the shadowgraph as was the case with suction. From this it appears the shock was exterior to the separated flow and formed at some distance from the model, possibly as a concentration of weaker waves that emanated from the separated flow. The shock does not intersect the model surface through the separated flow in figure 10(g); it appears to because of the essentially normal and three-dimensional nature of the shock.

Suction applied at either spacing of the hole rows was not capable of completely attaching the flow at 0.80 Mach number but marked changes in the shock pattern and higher peak negative pressure coefficients are evident as shown in figures 10(c) and 10(d), respectively. Whether the

changes in the flow were sufficient to give dynamic stability (see refs. 2 and 3) is not known but at a Mach number of 0.80, the shocks resemble those on the spherical-nosed model of reference 2 which was dynamically stable at this Mach number.

Correlation of Blunt Body Pressures

Inviscid transonic-flow theory, at present, is not capable of predicting or correlating pressure distributions of blunt axially symmetric bodies at transonic Mach numbers. The blunt models of this investigation and reference 2 do not fulfill the requirements set forth in theory (ref. 4 for example) wherein slender pointed configurations are essential in order that the boundary conditions at the model surface may be properly approximated. With complete disregard for rigor, the transonic similarity parameters of plane flow, $\frac{C_p[(\gamma + 1)M^2]^{1/3}}{\tau^{2/3}}$ and $\frac{1 - M^2}{[\tau(\gamma + 1)M^2]^{2/3}}$, were selected as a basis for empirically correlating the peak negative pressure coefficients of the models of this investigation and those of reference 2. The thickness ratio, τ, of the plane flow parameters was identified as nose thickness of the axisymmetric models and was replaced by $(\tau + \alpha)$ with α measured in radians in order to account for effects of angle of attack.

Although justified solely on the basis of expediency, plausible reasons can be given to warrant these substitutions. The selection of plane flow similarity parameters was influenced by the observation that the locally induced velocities on blunt axisymmetric bodies are considerably greater than on pointed axisymmetric bodies and are perhaps more nearly comparable to those for plane flow. Also, a certain equivalence exists between τ and α since increasing either τ or α increased the maximum negative pressure coefficient.

A plot of the peak negative pressure coefficient with attached flow obtained from this investigation and reference 2 is given in figure 11 with the modified plane flow similarity parameters as coordinates. Data with suction applied are also included for Mach numbers of 0.60, 0.90, and 0.94 since the flow was essentially attached. From this figure several interesting observations can be made. For Mach numbers greater than 1.00, good correlation was obtained at angles of attack from 0° to 20° and nose thicknesses of 1/2 and 1.0. Good correlation also exists at high subsonic Mach numbers for these nose thicknesses at low angles of attack but is poorer at high angles of attack. However, for a nose thickness of 2.0, the data do not correlate with the data for models with the lesser nose thicknesses. It is thus indicated that, even in

the absence of separation, the flow over an oblate-nosed model may differ basically from that over a less blunt model. It should be noted for all these data at Mach numbers near 1.00 that the variation of $\frac{C_{p_{max}}[(\gamma + 1)M^2]^{1/3}}{(\tau + \alpha)^{2/3}}$ with $\frac{1 - M^2}{[(\tau + \alpha)(\gamma + 1)M^2]^{2/3}}$ was linear and had the same slope for all nose thicknesses.

Also, for all nose thicknesses, the peak negative value of $\frac{C_{p_{max}}[(\gamma + 1)M^2]^{1/3}}{(\tau + \alpha)^{2/3}}$ was about 1.4. For nose thicknesses of 1.0 or less, the peak occurred at a value of $\frac{1 - M^2}{[(\tau + \alpha)(\gamma + 1)M^2]^{2/3}}$ of about 0.2, thus affording a rapid approximate estimate of the maximum negative value of $C_{p_{max}}$ for a specified nose thickness and angle of attack. If the nose thickness was greater than 1.0, interpolation or extrapolation is required to determine at what value of $\frac{1 - M^2}{[(\tau + \alpha)(\gamma + 1)M^2]^{2/3}}$ the peak occurred (see fig. 11).

A 3 9 1

Angle of Attack for Separation

An empirical method of estimating the angle of attack for separation of ellipsoidal-nosed cylinder-flare models at transonic Mach numbers is derived in the appendix. The method is based on the linear relation existing between the similarity parameters of figure 11 for Mach numbers near 1.0 and fitting a power curve to separation boundaries. The results, presented in figure 12, show the variation with Mach number of angle of attack for separation normalized with respect to nose thickness. Shown for comparison are angles of attack for separation determined from the pitching-moment data of references 1 and 2. In general, the experimental values determined from the pitching-moment data agree with the empirical estimate. The generally lower values of the experimental data at Mach numbers near 1.1 are believed due to the reflection of disturbances from the tunnel walls striking the model as discussed in reference 1. Since Reynolds number is an important parameter in the transonic separation phenomena, the results are believed applicable mainly for Reynolds numbers approximating those of this investigation. Moreover, unpublished data as well as the data of reference 2 indicate the results may not apply to configurations having longer flares or other flare angles.

CONCLUDING REMARKS

Tests of oblate ellipsoidal-nosed cylinder-flare models have shown that separation of the flow may occur at subcritical Mach numbers at 0° angle of attack if the nose is sufficiently blunt. Although decreasing nose bluntness eliminated subcritical separation, the formation of local shocks induced separation at supercritical Mach numbers for the less blunt model tested. The application of a small amount of suction locally near the nose-body juncture was capable of controlling the boundary layer sufficiently to prevent shock-induced separation at Mach numbers greater than about 0.90. Although suction did not prevent separation at a Mach number of 0.80, significant changes in the shock pattern and pressure distribution were observed.

Peak negative pressure coefficients of the models having attached flow were empirically correlated at Mach numbers near 1.0 with the plane flow transonic similarity parameters as coordinates. With the aid of experimental separation boundaries obtained from peak negative pressure coefficients the correlation allowed an estimate to be made of the angle of attack for transonic flow separation.

Ames Research Center
National Aeronautics and Space Administration
Moffett Field, Calif., March 3, 1961

APPENDIX

ESTIMATION OF ANGLE OF ATTACK FOR SEPARATION

A procedure for estimating the angle of attack for separation of ellipsoidal-nosed cylinder-flare models at transonic Mach numbers was developed by empirically fitting a power curve to separation boundaries. The separation boundaries were determined experimentally from pressure distributions of this investigation and reference 2 and represent the peak negative pressure coefficient that can be achieved by increasing the angle of attack before flow separation ensues. Since the slope of the boundary was always less than the curves representing the variation of $C_{p_{max}}$ at constant angle of attack with Mach number as shown by sketch (b), the intersection of the boundary with the curves of $C_{p_{max}}$ uniquely determines the angle of attack for transonic separation.

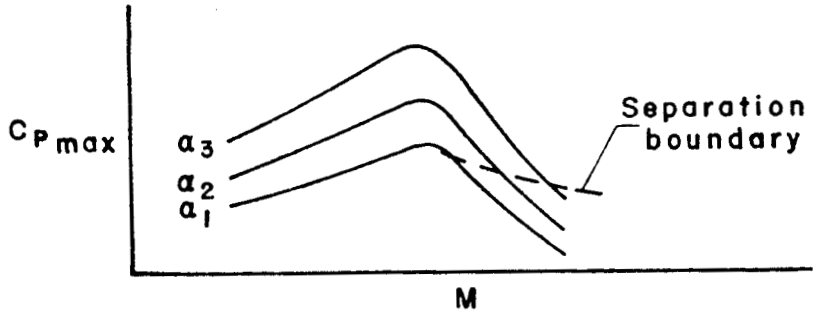

Sketch (b)

The correlation of $C_{p_{max}}$ presented in figure 11 provides an expression for $C_{p_{max}}$ as a function of M, α, and τ within the Mach number and angle-of-attack range of interest. If $C_{p_{max}}$ is assumed negative, the linear portion of the curves of figure 11 is:

$$\frac{C_{p_{max}}[(\gamma + 1)M^2]^{1/3}}{(\tau + \alpha)^{2/3}} = m\left\{\frac{1 - M^2}{[(\tau + \alpha)(\gamma + 1)M^2]^{2/3}} - a\right\} + b \qquad (1)$$

The slope, m, and intercept, b, have the values 1.43 and 1.12, respectively, while a allows for the horizontal displacement of the curves for $\tau = 2$ and $\tau = 1/2$ and 1. For nose thickness of 1/2 and 1.0, $a = 0$; for thicknesses of 2.0, $a = 0.18$.

The separation boundary was approximately represented by the curve

$$C_{p_s} = \frac{C_{p_s}^*}{M^{3/2}} \tag{2}$$

where $C_{p_s}^*$ was the value of C_{p_s} for $M = 1.0$. The values of $C_{p_s}^*$ for models having nose thicknesses of 1 and 2 were 0.90 and 1.05, respectively (see ref. 2, fig. 24). At the intersection of the separation boundary with the curves of $C_{p_{max}}$ (sketch (b))

$$C_{p_s} = C_{p_{max}} \text{ and } \alpha_s = \alpha$$

A 3 9 1

After substitution and algebraic manipulation, α_s normalized with respect to τ is given by

$$\frac{\alpha_s}{\tau} = \frac{1}{\tau}\left\{\frac{C_{p_s}^*(\gamma+1)^{1/3}}{(b - ma)}\frac{1}{M^{5/6}} - \frac{m}{(b - ma)(\gamma + 1)^{2/3}}\frac{1 - M^2}{M^{4/3}}\right\}^{3/2} - 1 \tag{3}$$

[redacted]

REFERENCES

1. Reese, David E., Jr., and Wehrend, William R., Jr.: An Investigation of the Static and Dynamic Aerodynamic Characteristics of a Series of Blunt-Nosed Cylinder-Flare Models at Mach Numbers From 0.65 to 2.20. NASA TM X-110, 1960.

2. Cleary, Joseph W.: The Effects of Nose Bluntness on the Flow Separation and Longitudinal Characteristics of Ellipsoidal-Nosed Cylinder-Flare Models at Transonic Speeds. NASA TM X-370, 1960.

3. Emerson, Horace F., and Robinson, Robert C.: The Transonic Damping in Pitch of Three Cylinder-Flare Models With Various Degrees of Nose Bluntness. NASA TM X-368, 1960.

4. Spreiter, John R., and Alksne, Alberta Y.: Slender-Body Theory Based on Approximate Solution of the Transonic Flow Equation. NASA Rep. R-2, 1959.

[redacted]

TABLE I.- PRESSURE ORIFICE LOCATION

τ = 2 Oblate-nosed model		τ = 4 Oblate-nosed model	
r/(d/2)	x/l	r/(d/2)	x/l
0	0	0	0
.186	.038	.158	.034
.478	.114	.386	.067
.658	.189	.553	.100
.816	.265	.713	.134
.895	.340	.822	.215
.954	.416	.878	.282
.987	.492	.922	.349
1.000	.567	.954	.416
	.642	.983	.482
	.741	1.000	.550
	.804		.616
	.876		.684
	.949		.770
			.826
			.890
			.954

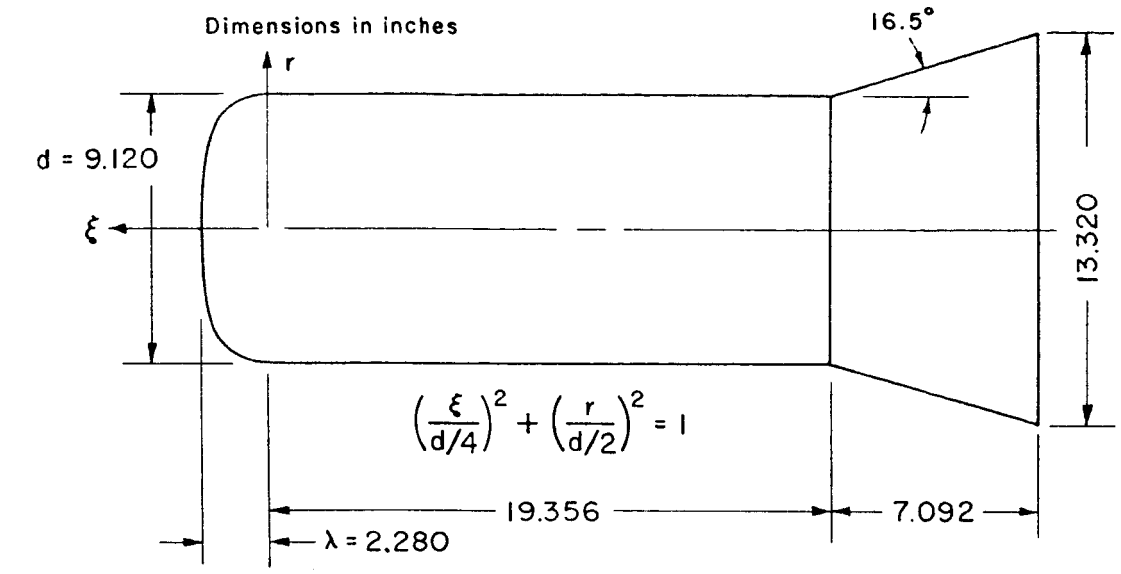

(a) $\tau = 2$ oblate-nosed cylinder-flare model (ref. 2).

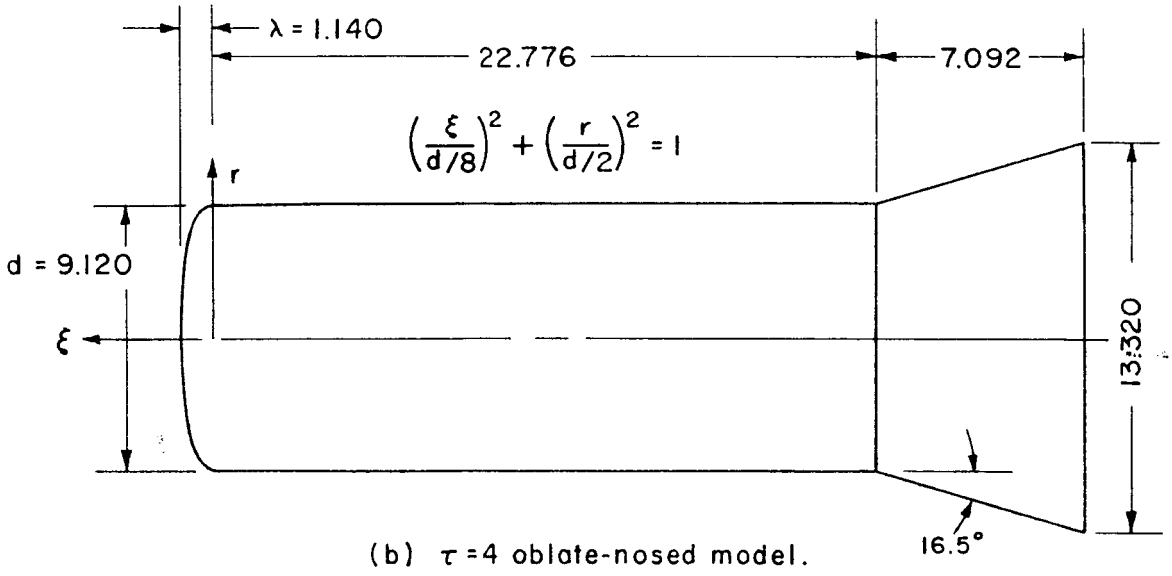

(b) $\tau = 4$ oblate-nosed model.

Figure 1.- Dimensional details of the models.

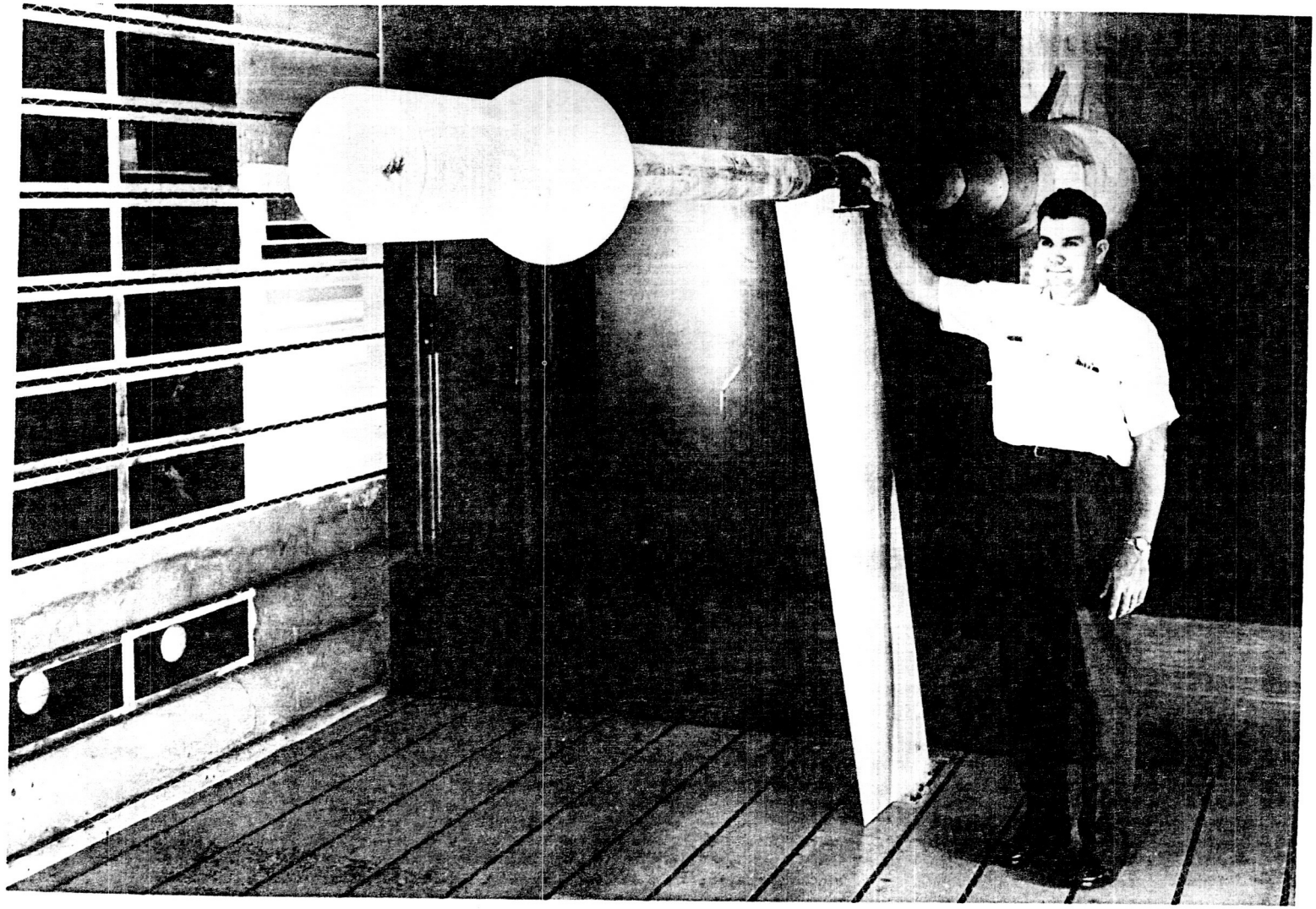

A-25729

Figure 2.- Model installation for tests with suction.

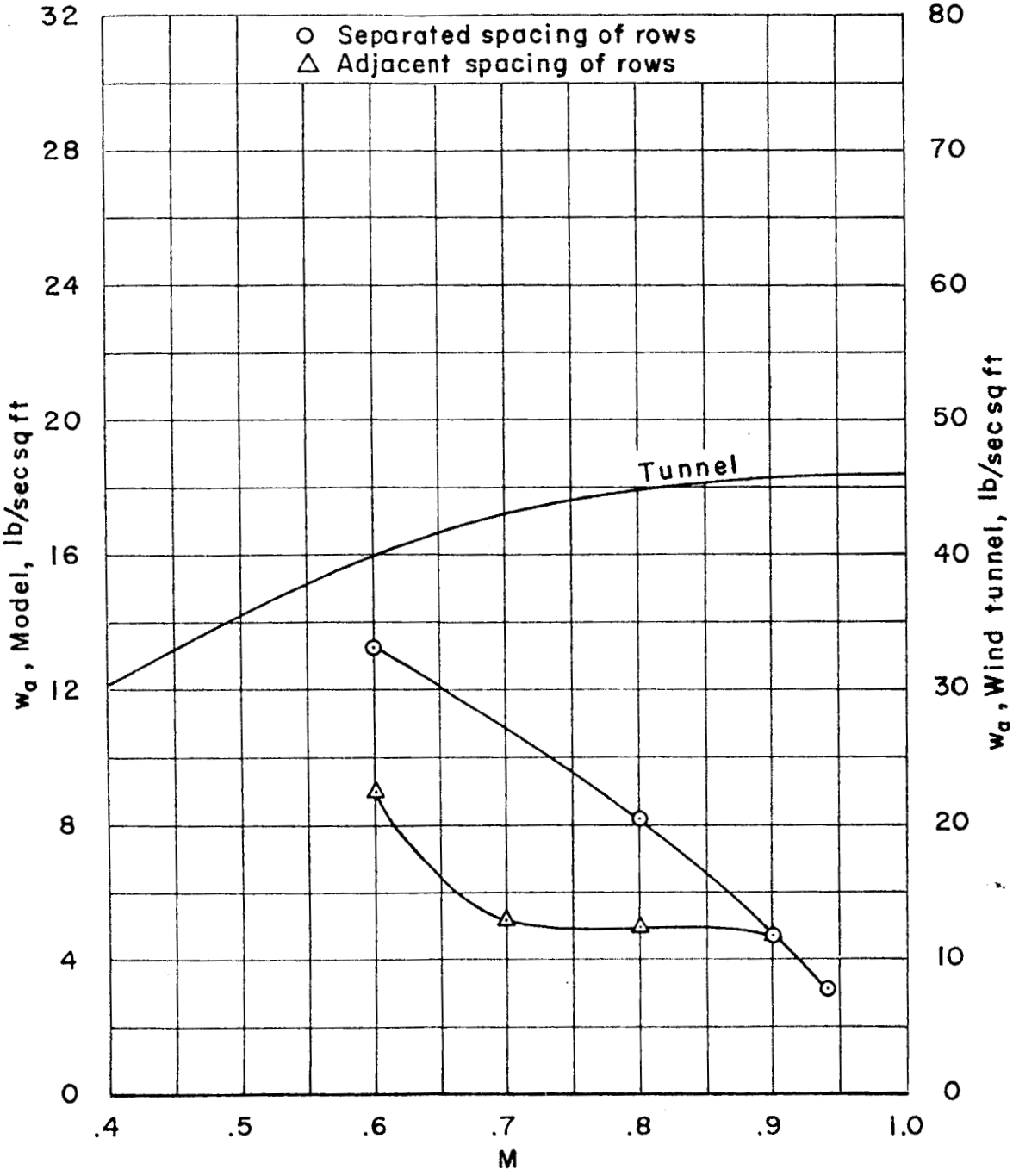

Figure 3.- Air mass flow rates of the wind tunnel and the $\tau = 2$ model with suction.

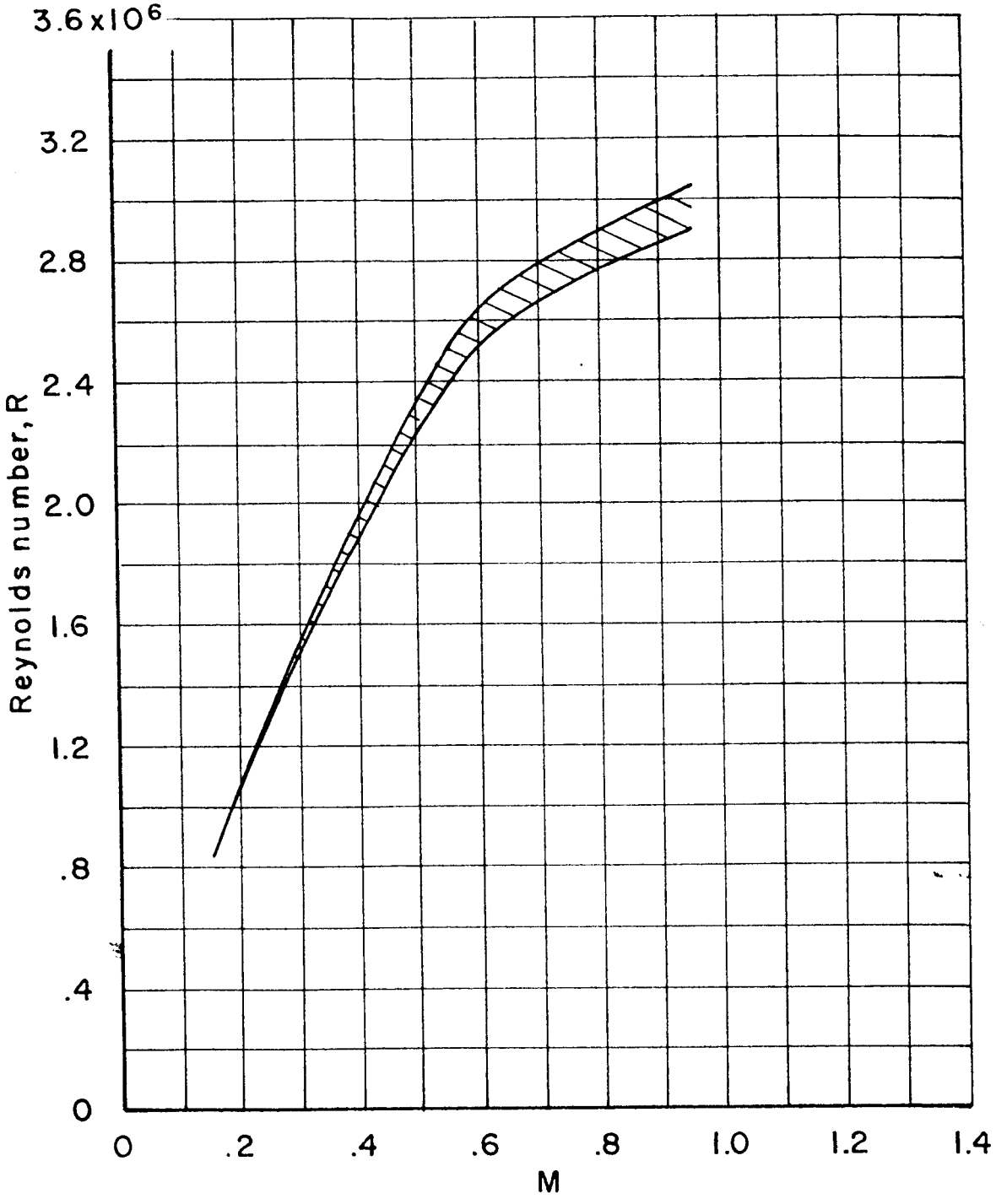

Figure 4.- Reynolds number range of the tests.

A
3
9
1

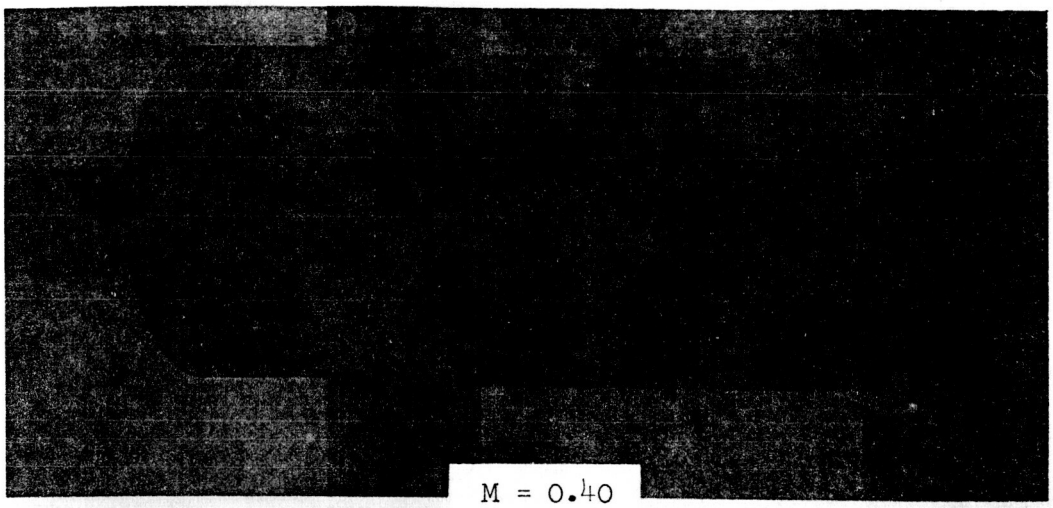

M = 0.40

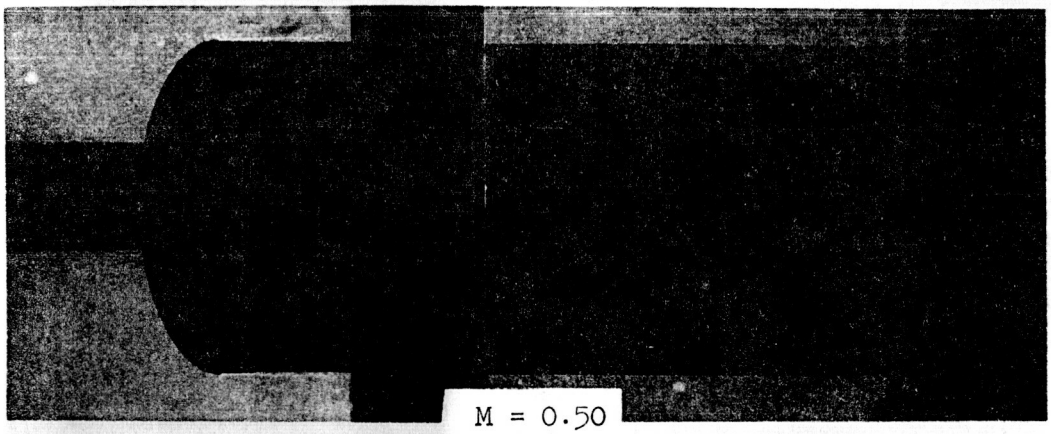

M = 0.50

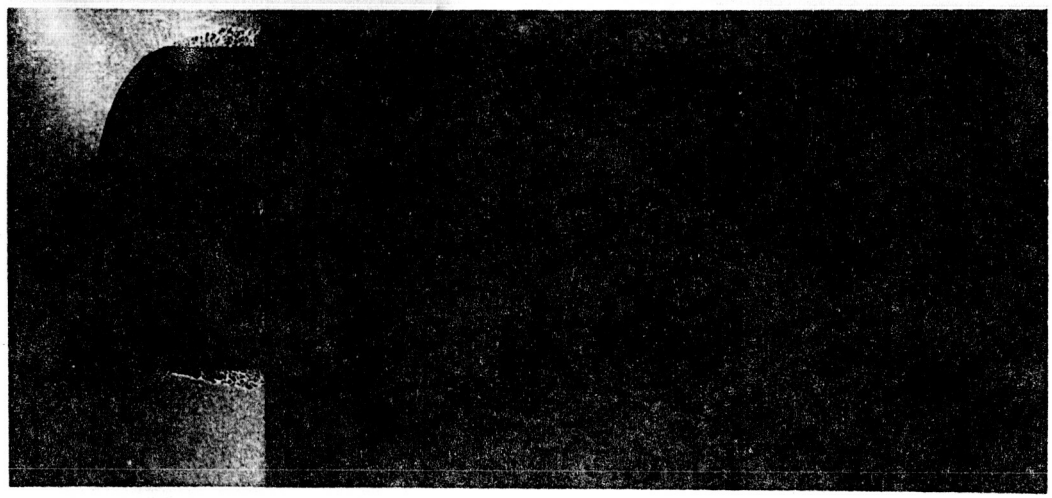

M = 0.60

(a) Shadowgraph, $\alpha = 0^{\circ}$.

Figure 5.- Effect of Mach number on the flow and pressure distribution of the $\tau = 2$ model.

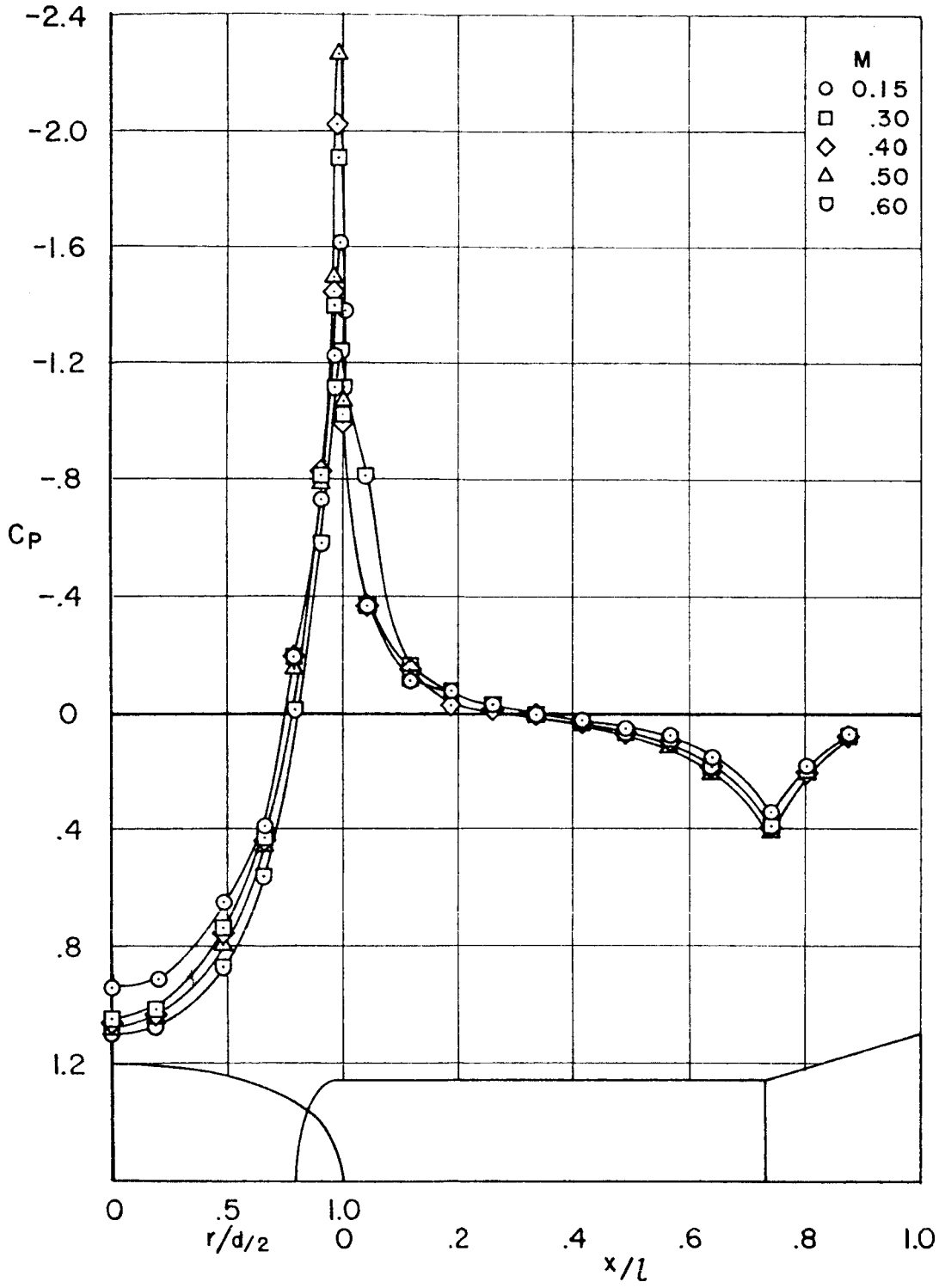

(b) Pressure distribution, $\alpha = 0^{\circ}$.

Figure 5.- Concluded.

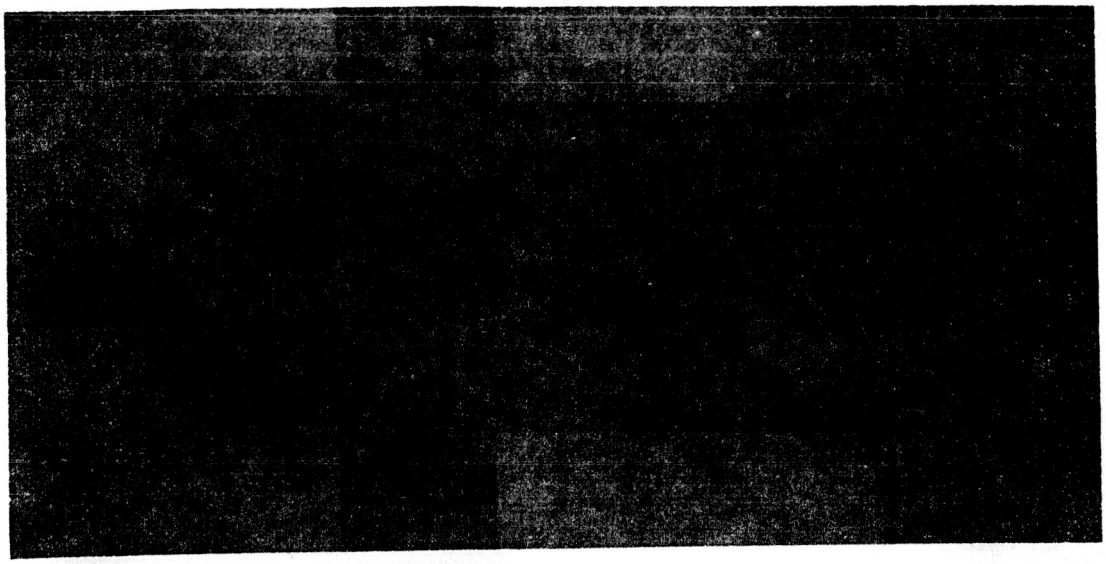

$\alpha = 0^{\circ}$

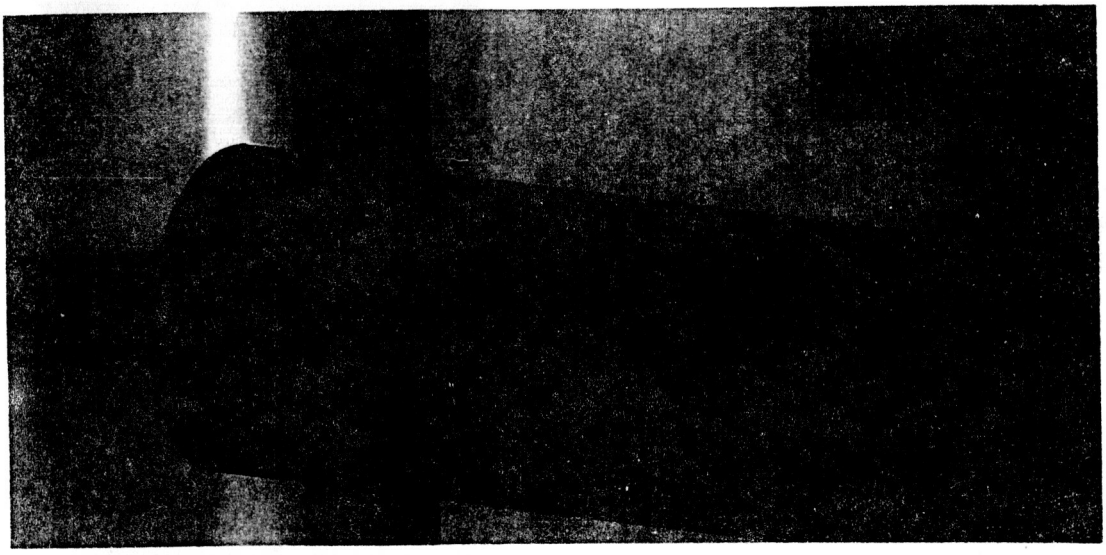

$\alpha = 8^{\circ}$

(a) Shadowgraph, M = 0.40.

Figure 6.- Effect of angle of attack on the flow and pressure distribution of the $\tau = 2$ model.

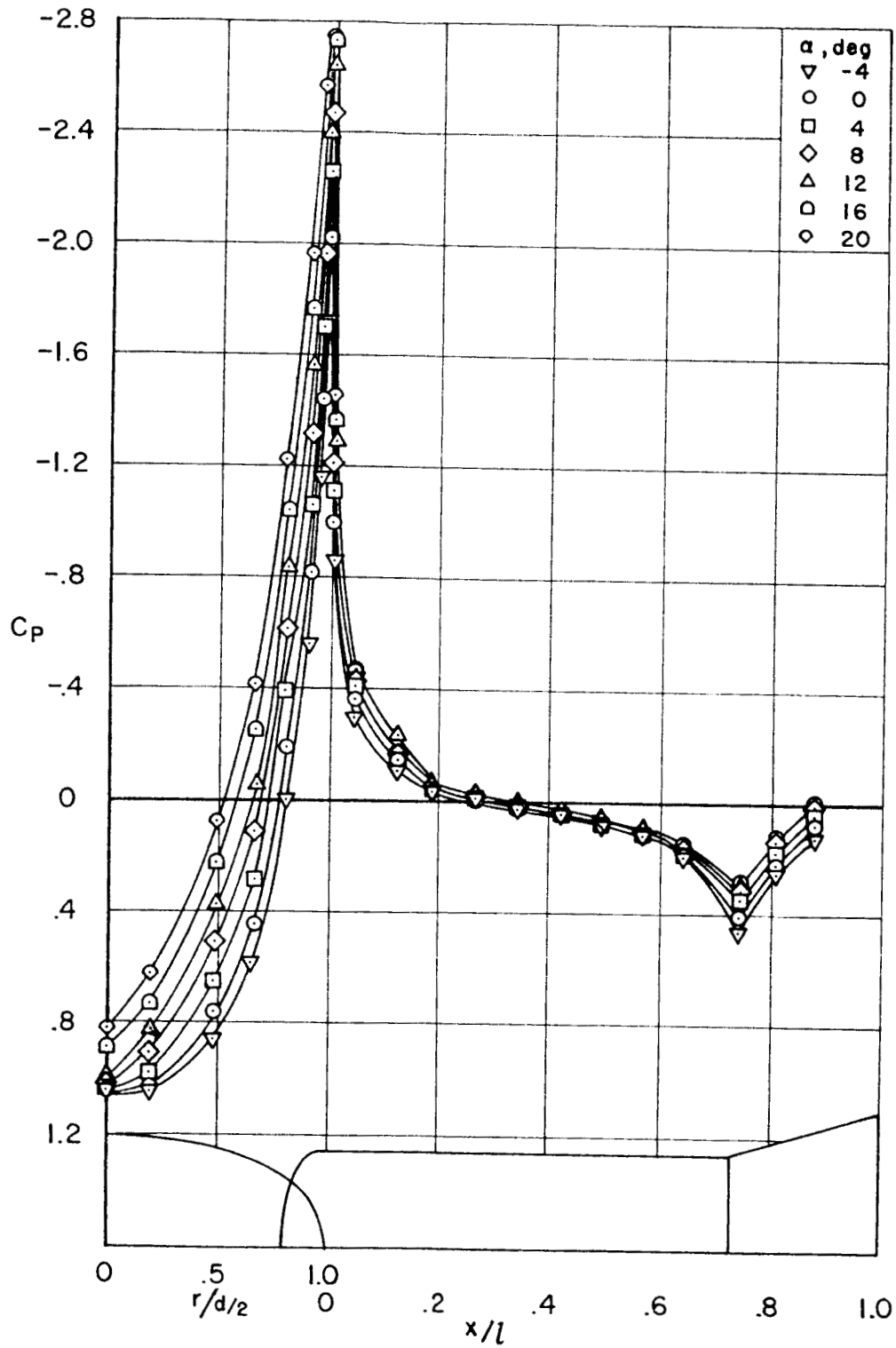

(b) Pressure distribution, M = 0.40.

Figure 6.- Concluded.

[redacted]

[redacted]

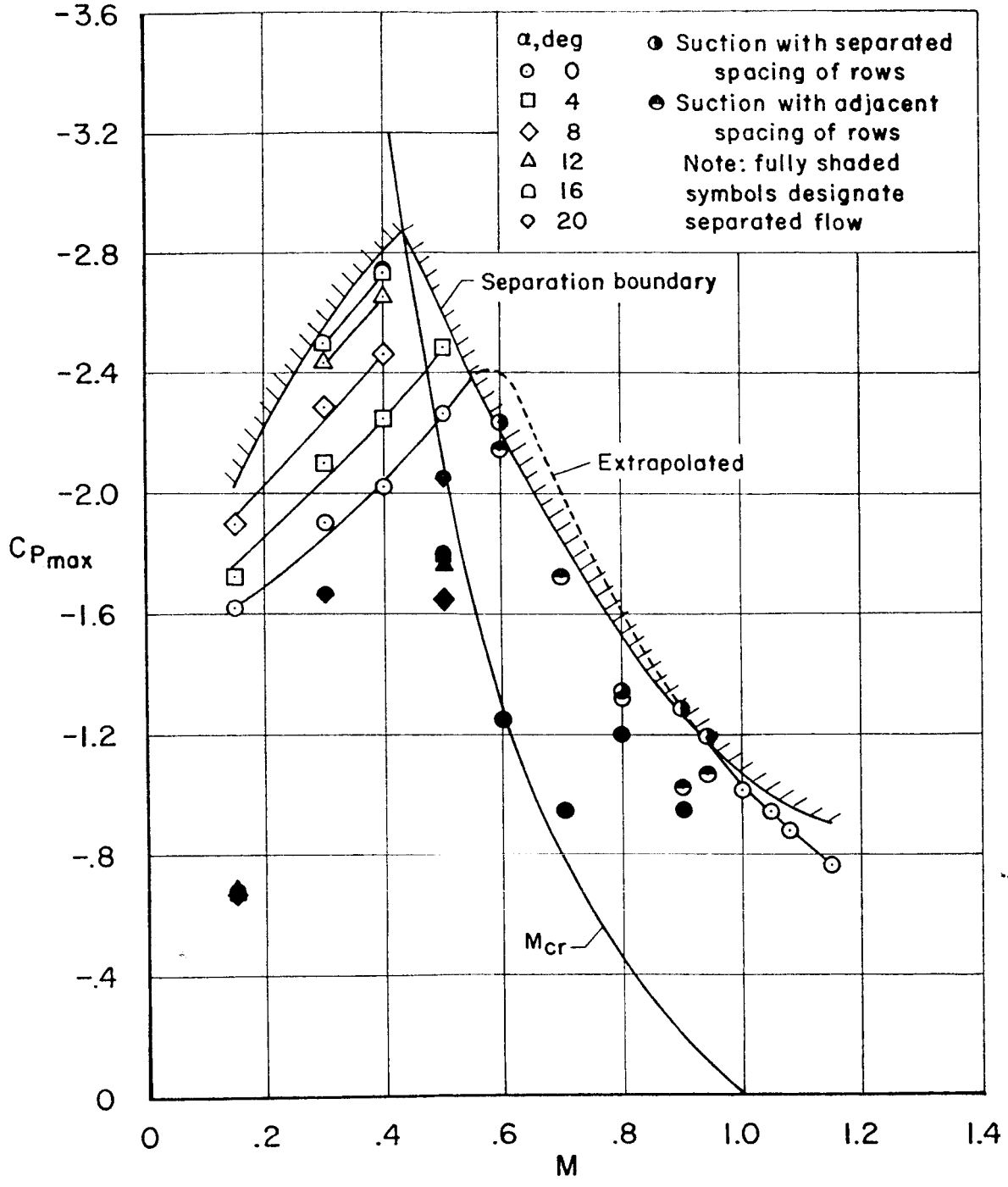

Figure 7.- Variation of maximum negative pressure coefficient of the $\tau = 2$ model with Mach number.

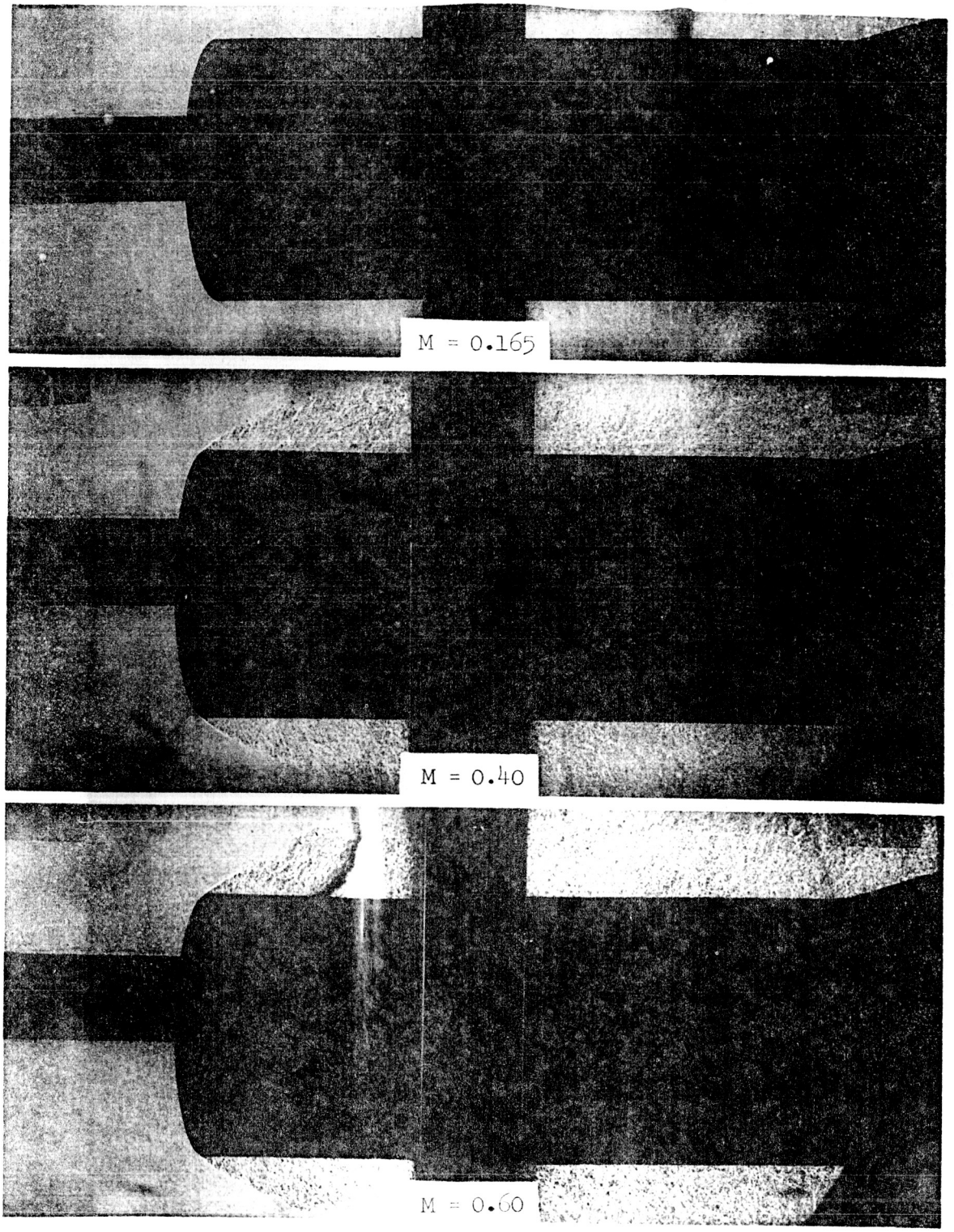

(a) Shadowgraph, $\alpha = 0^{\circ}$.

Figure 8.- Effects of Mach number on the flow and pressure distribution of the $\tau = 4$ model.

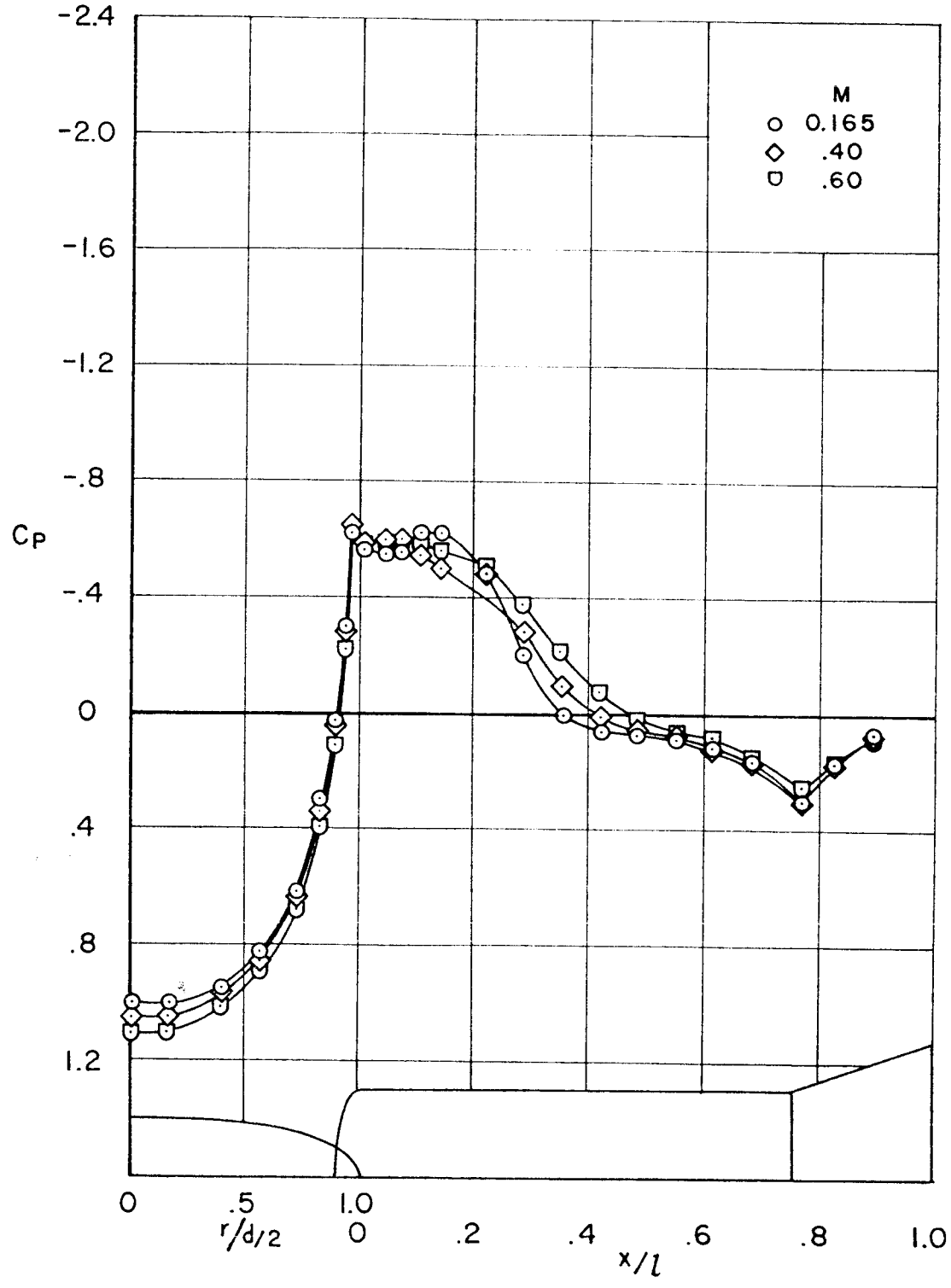

(b) Pressure distribution, $\alpha = 0^{\circ}$.

Figure 8.- Concluded.

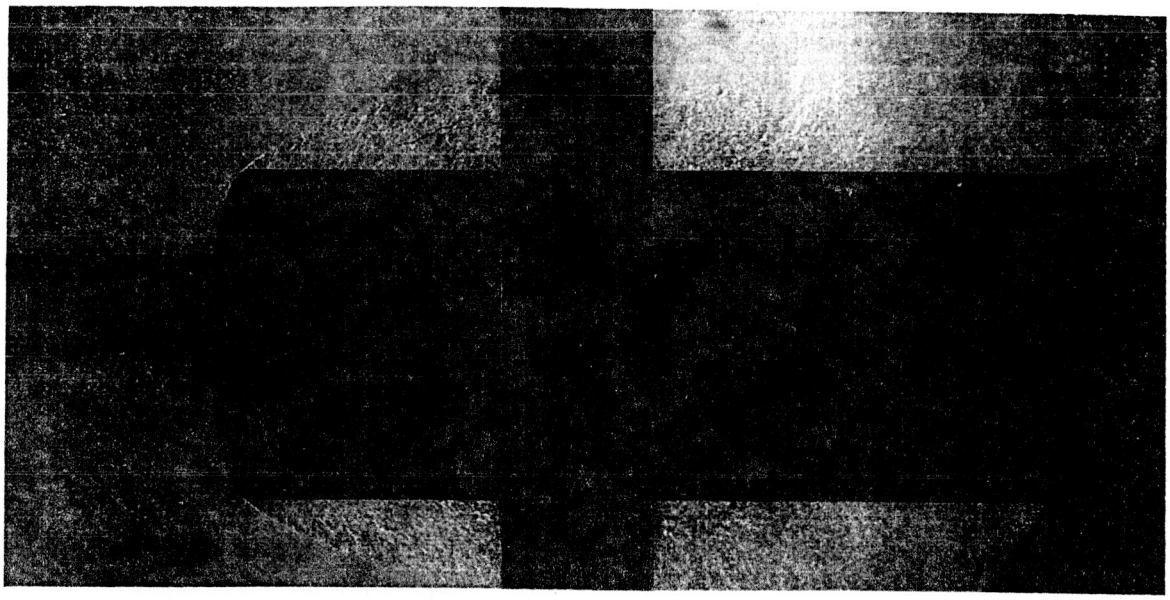

$\alpha = 0^{\circ}$

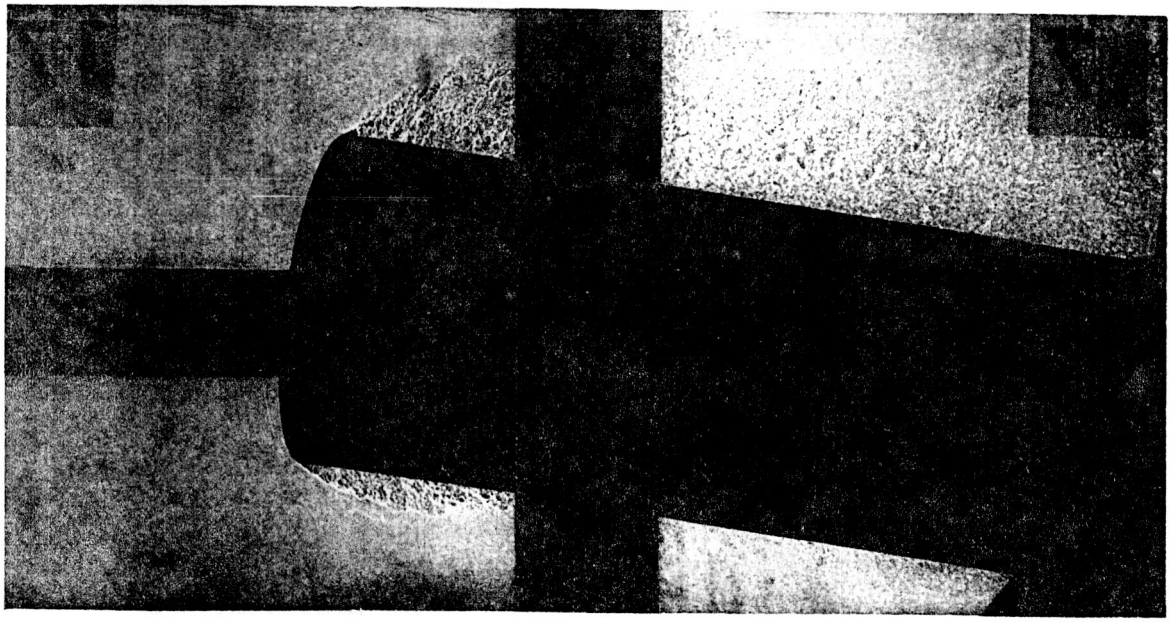

$\alpha = 8^{\circ}$

(a) Shadowgraph, M = 0.40.

Figure 9.- Effect of angle of attack on the flow and pressure distribution of the $\tau = 4$ model.

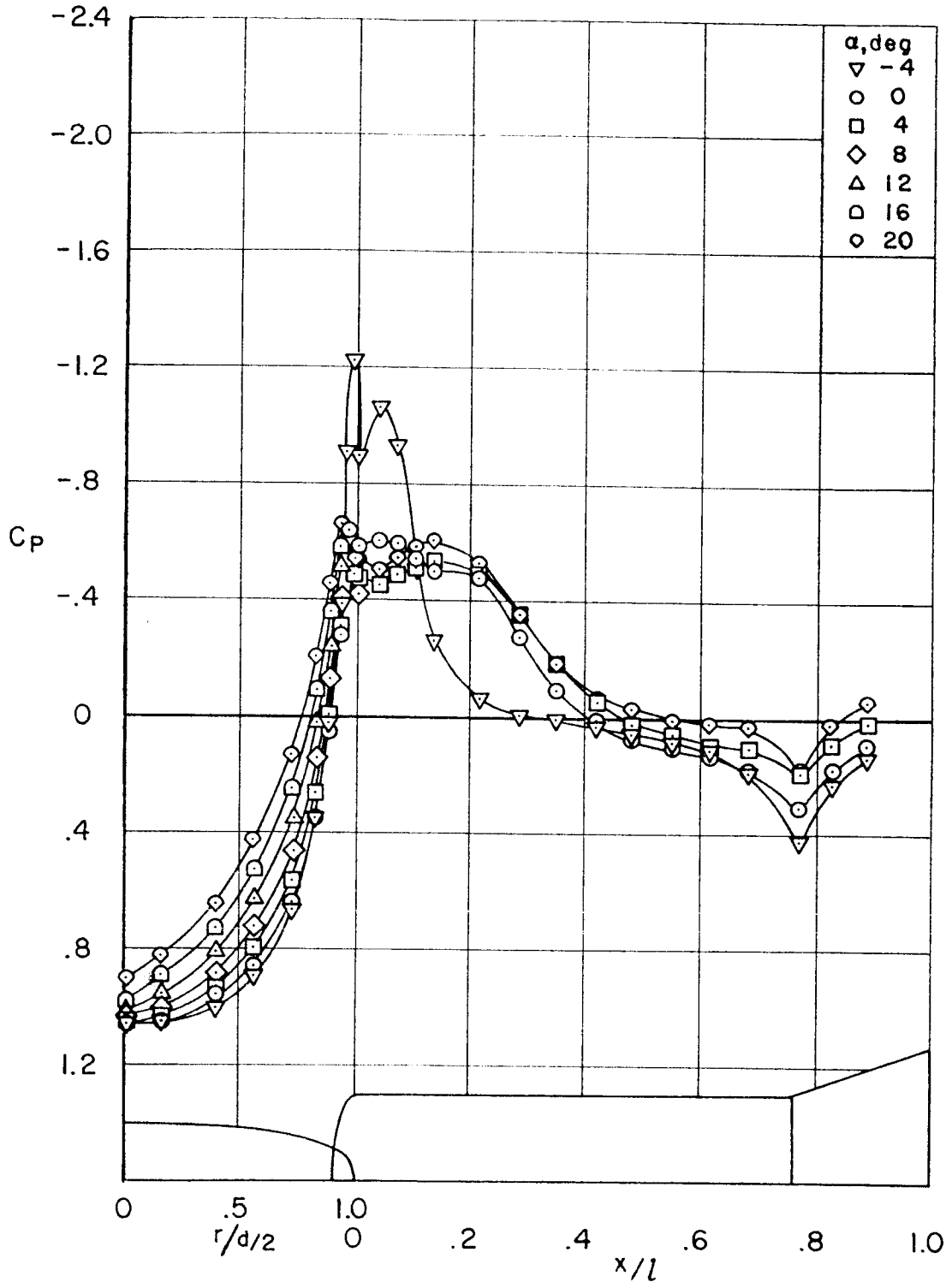

(b) Pressure distribution, M = 0.40.

Figure 9.- Concluded.

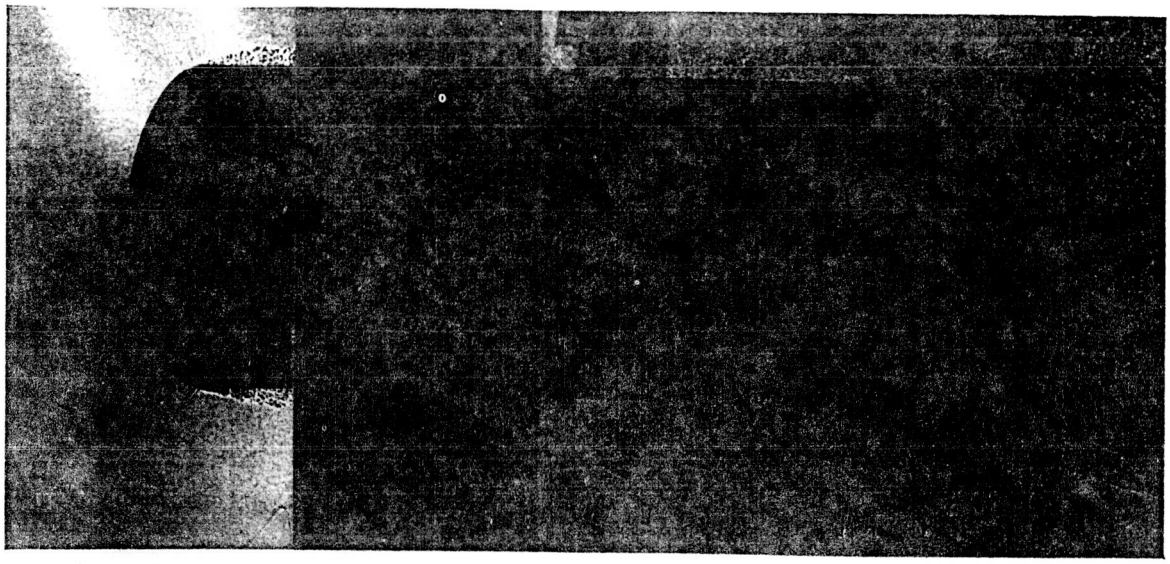

Without suction.

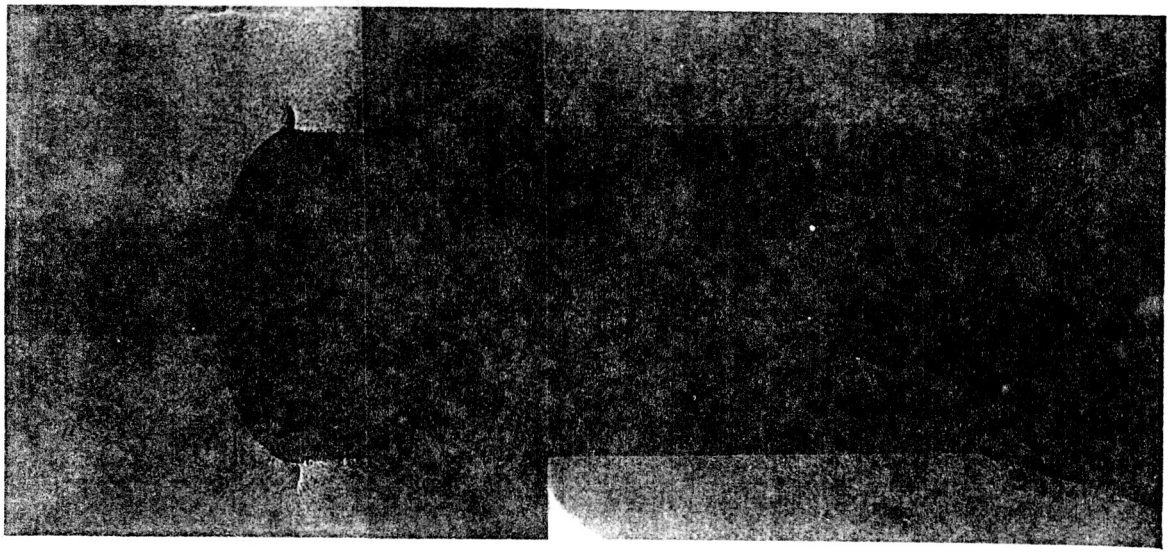

With suction at separated spacing of rows.

(a) Shadowgraph, M = 0.60.

Figure 10.- The effect of suction on the flow and pressure distribution of the $\tau = 2$ model.

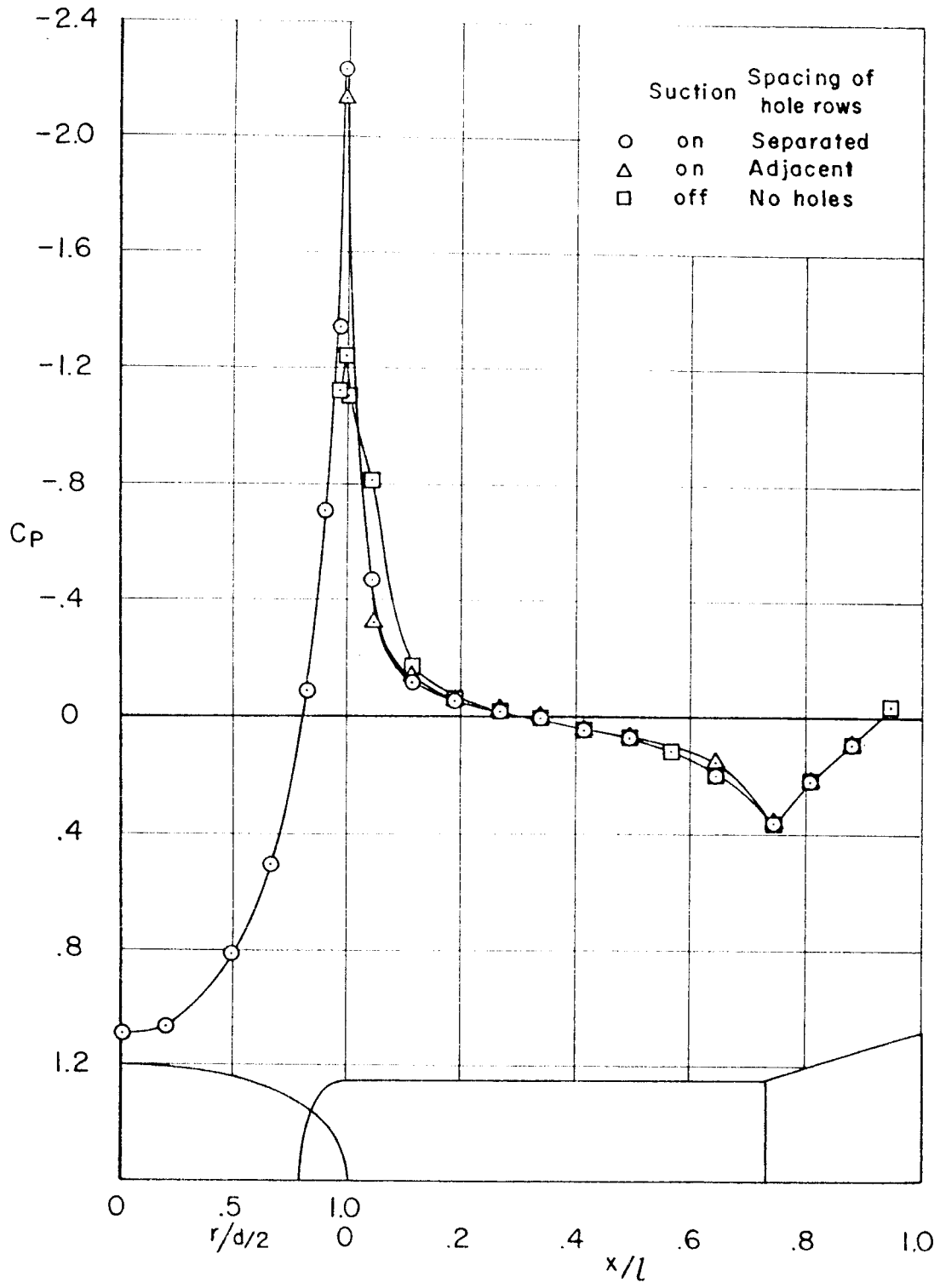

(b) Pressure distribution, M = 0.60.

Figure 10.- Continued.

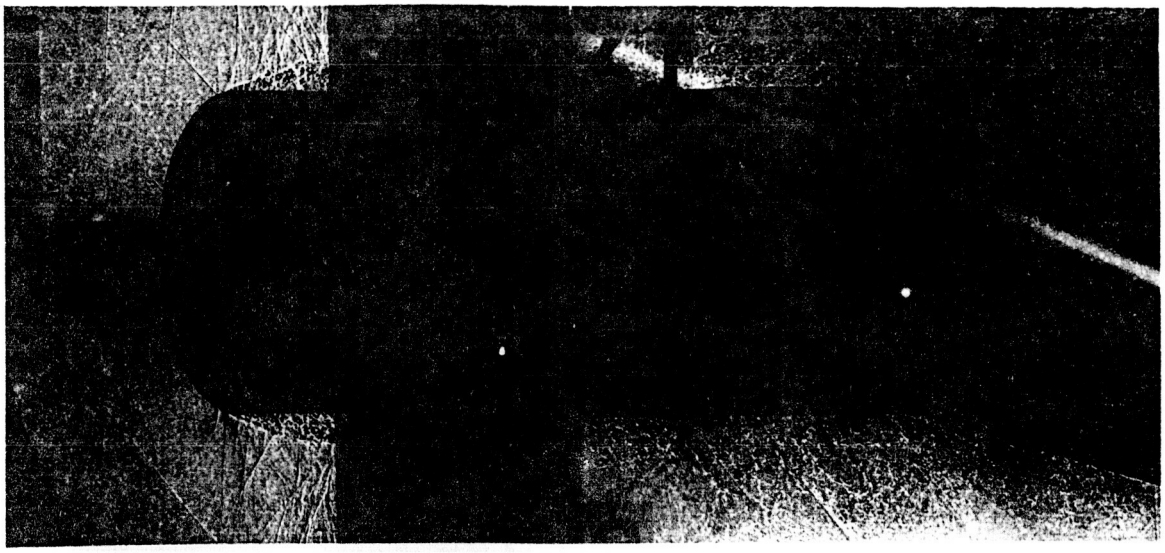

Without suction.

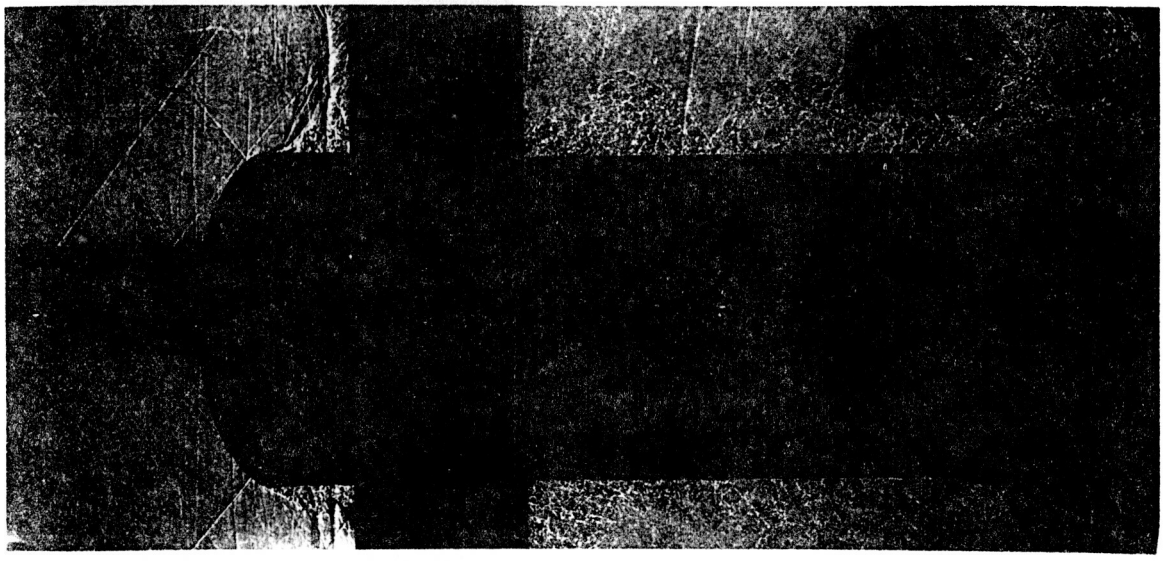

With suction at separated spacing of rows.

(c) Shadowgraph, M = 0.80.

Figure 10.- Continued.

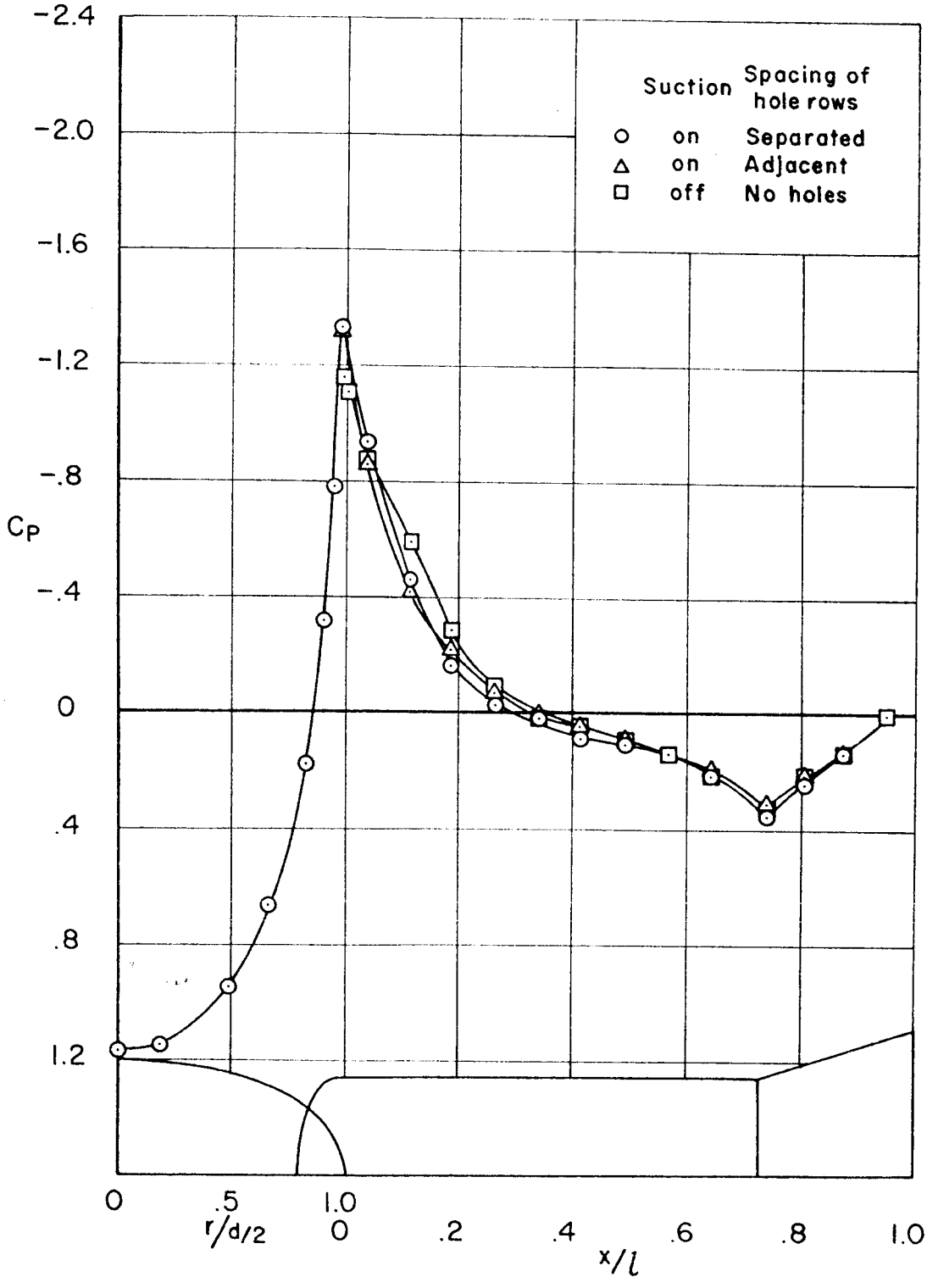

(d) Pressure distribution, M = 0.80.

Figure 10.- Continued.

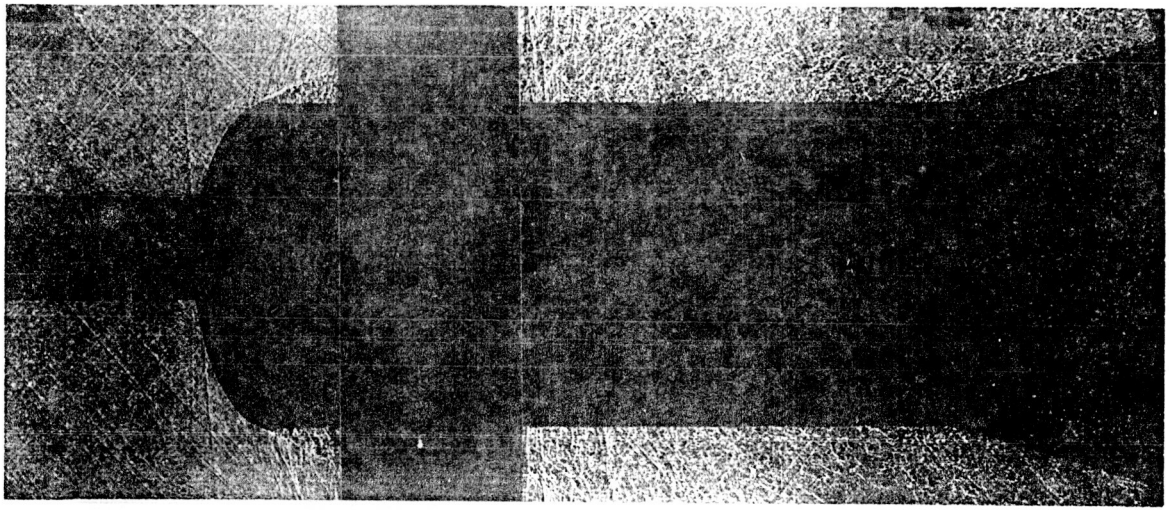

Without suction.

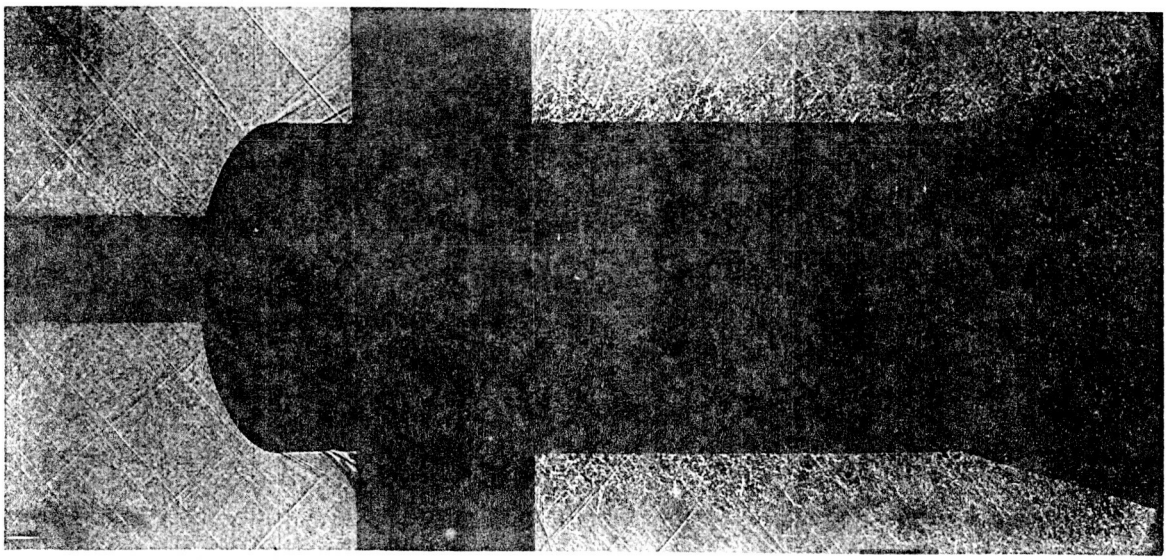

With suction at separated spacing of rows.

(c) Shadowgraph. M = 0.90.

Figure 10.- Continued.

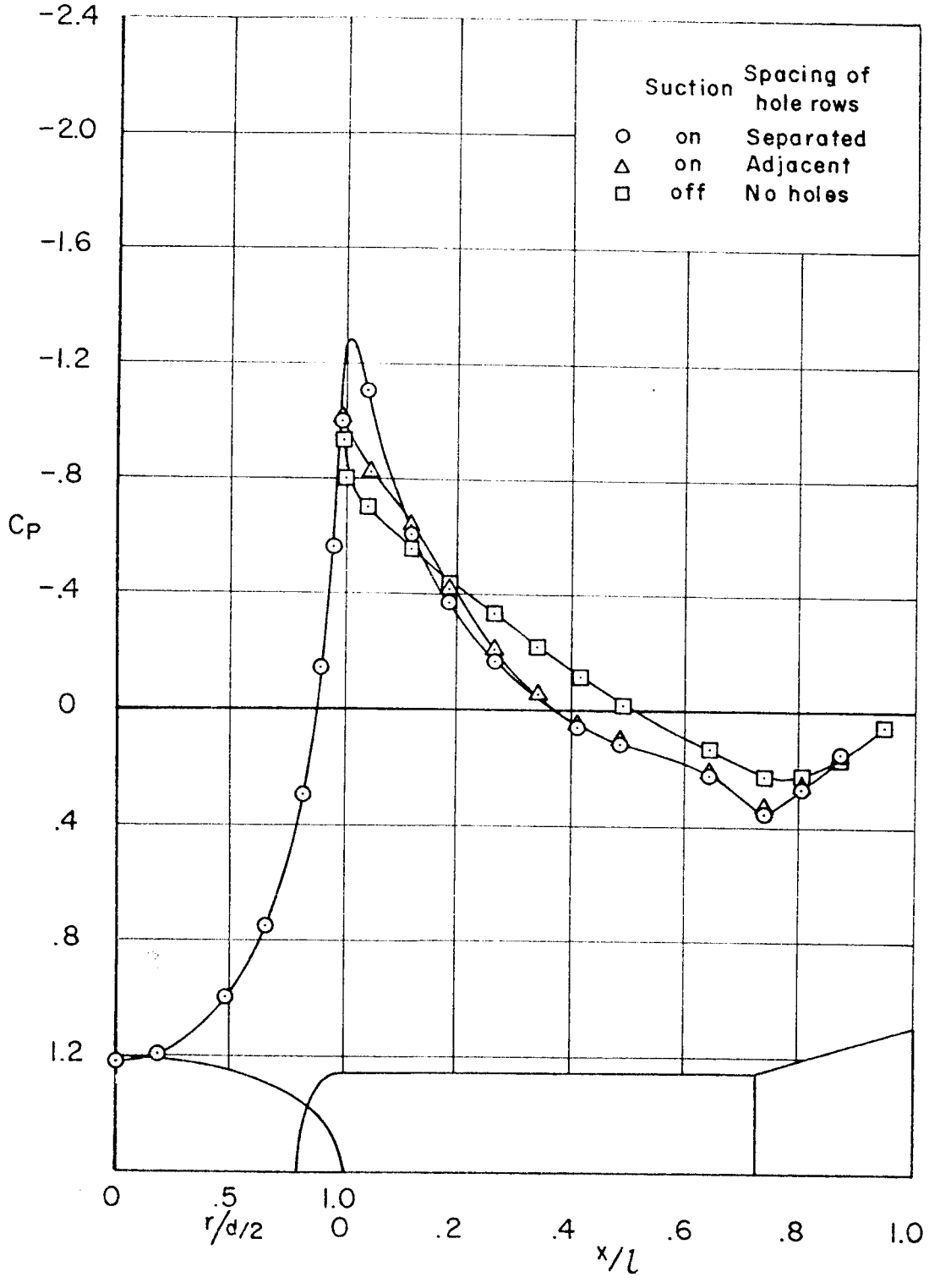

(f) Pressure distribution, M = 0.90.

Figure 10.- Continued.

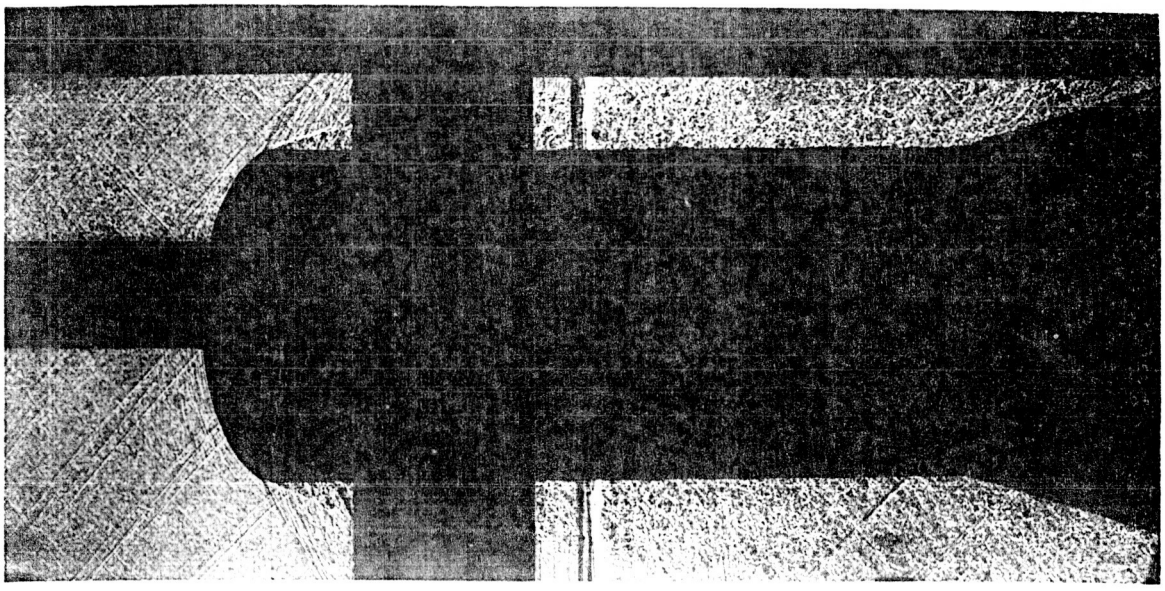

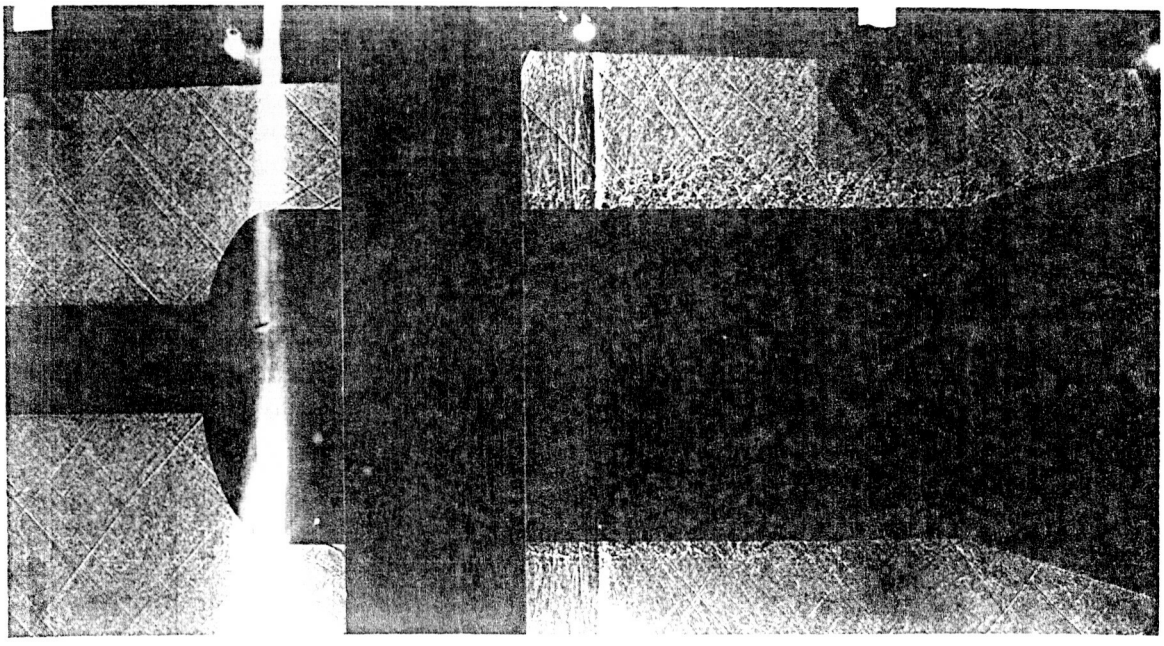

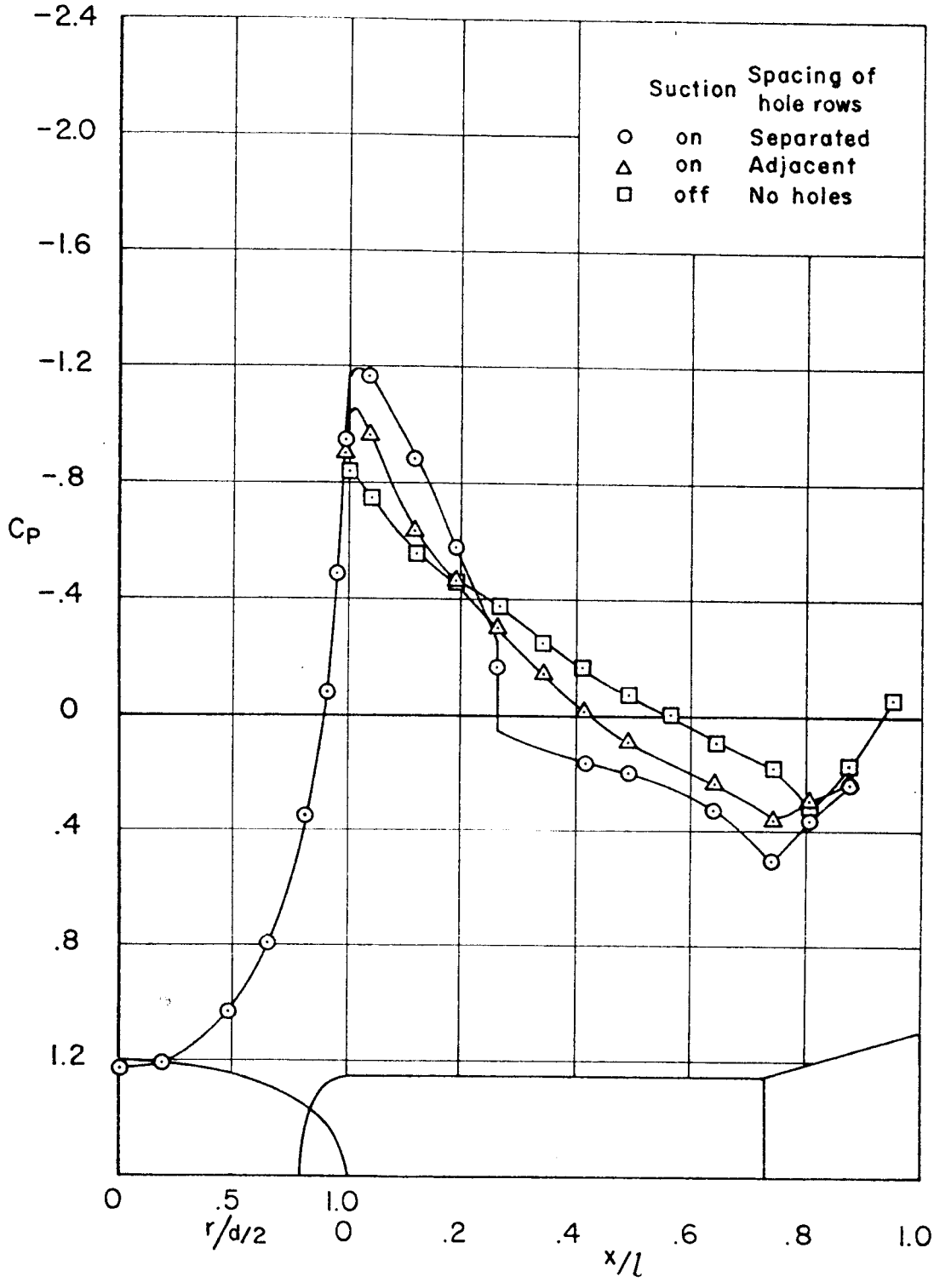

(h) Pressure distribution, M = 0.94.

Figure 10.- Concluded.

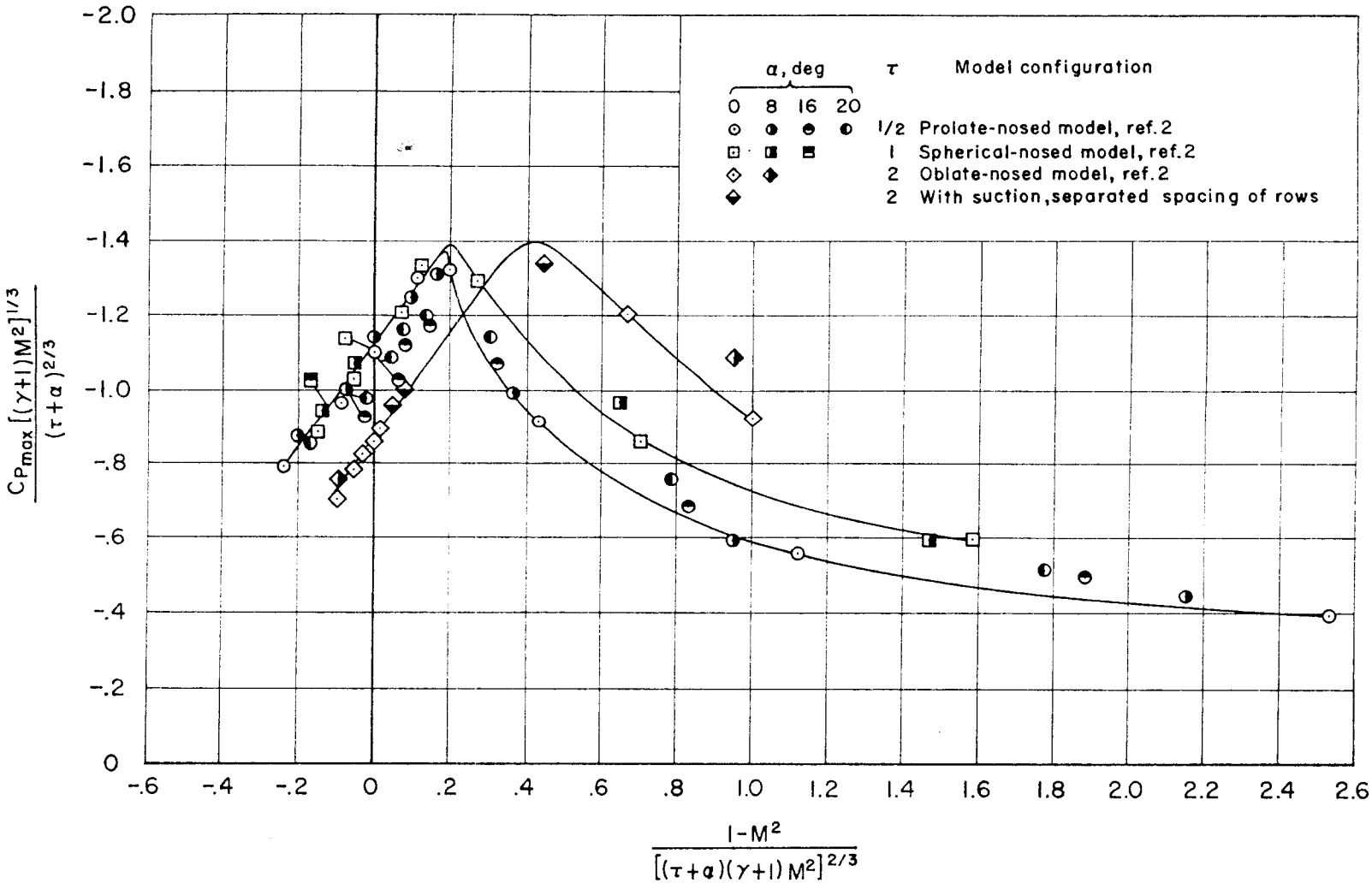

Figure 11.- Correlation of maximum negative pressure coefficient of ellipsoidal-nosed cylinder-flare models.

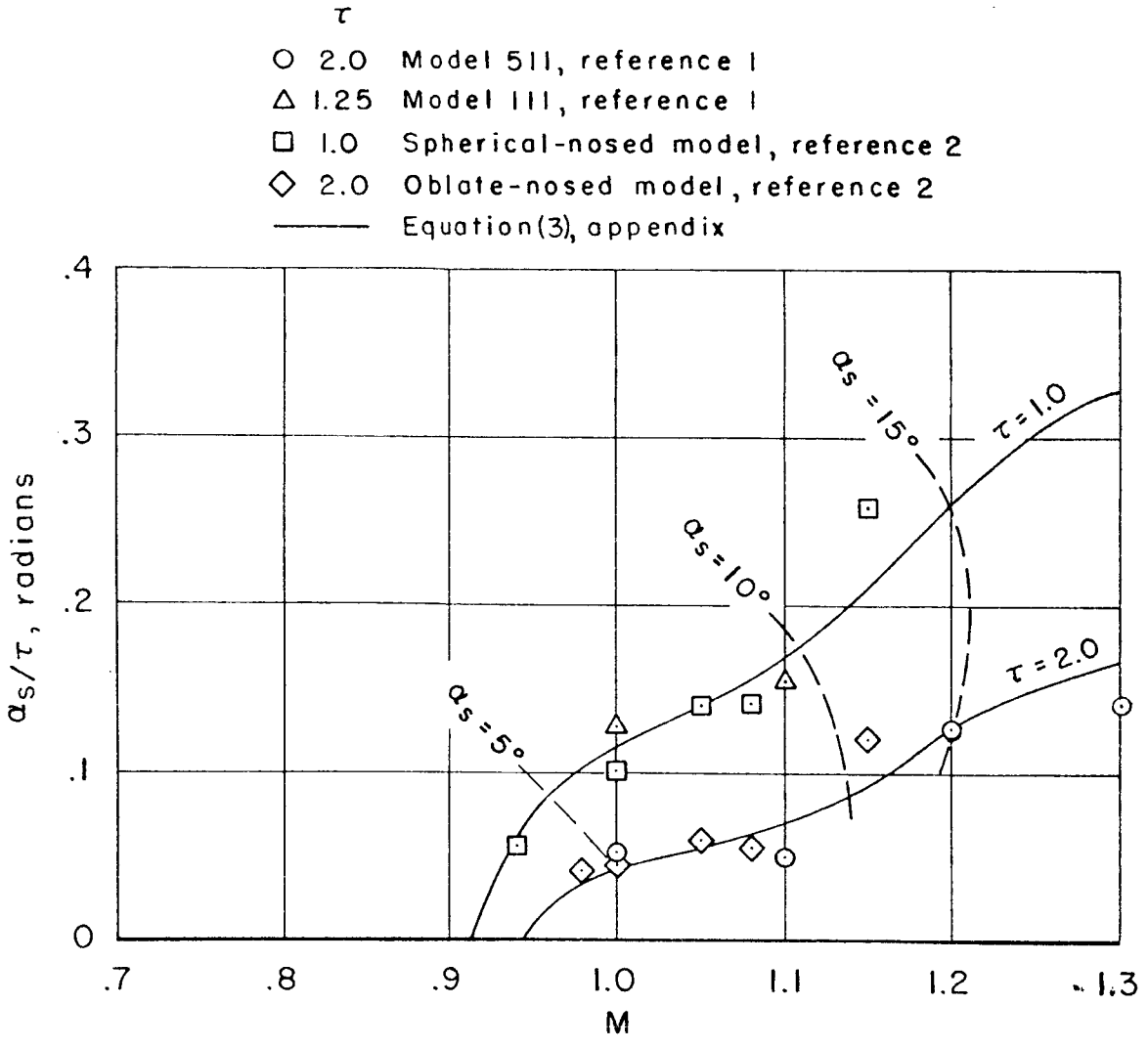

Figure 12.- Angle of attack for separation of ellipsoidal-nosed cylinder-flare models.